The effect of Pt/Pd ratio on the oxidation activity and resistance to sulfur poisoning for Pt-Pd/BEA diesel oxidation catalysts with high siliceous

Journal of Environmental Chemical Engineering 10 (2022) 108217

Contents lists available at ScienceDirect

Journal of Environmental Chemical Engineering

journal homepage: www.elsevier.com/locate/jece

The effect of Pt/Pd ratio on the oxidation activity and resistance to sulfur poisoning for Pt-Pd/BEA diesel oxidation catalysts with high siliceous content

Phuoc Hoang Ho *, Jieling Shao, Dawei Yao, Rojin Feizie Ilmasani, Muhammad Abdus Salam, Derek Creaser, Louise Olsson *

Chemical Engineering, Competence Centre for Catalysis, Chalmers University of Technology, SE-412 96 Gothenburg, Sweden

ARTICLE INFO

Editor: Dong–Yeun Koh

Keywords:
Diesel oxidation catalysts
PtPd alloy
Pt/Pd ratios
Sulfur poisoning
High siliceous zeolites

ABSTRACT

This study investigates the effect of the Pt/Pd ratio on the oxidation activity and sulfur poisoning/regeneration of diesel oxidation catalysts (DOC) using beta zeolites with high siliceous content as support. Formation of Pt-Pd alloy leads to contraction of the cell lattice of Pt in the bimetallic catalysts, improving not only the sintering resistance of Pt but also retaining a high fraction of Pd in Pd^{2+} form. Moreover, the Pt-Pd alloy also improves the oxidation resistance of the particles, which enhances the activity of the catalysts for CO and C_3H_6 oxidation. Bimetallic catalysts also favor NO reduction at a lower temperature than the monometallic Pt although they showed lower values for the absolute conversion of NO due to a decrease in the total number of the Pt active sites. In addition, the bimetallic catalysts significantly improved the sulfur resistance as compared to the monometallic Pd catalyst. Moreover, the bimetallic catalysts could easily recover their activity for NO and C_3H_6 oxidation by thermal treatment either in lean conditions or in H_2. The reduction with H_2 was necessary to recover completely the activity of the CO and C_3H_8 oxidation.

1. Introduction

Diesel oxidation catalysts (DOCs) play a key role in the emission control system of diesel vehicles [1]. Apart from its original functions, i.e. the removal of CO and unburnt hydrocarbons, modern DOCs are also important for NO oxidation to produce NO_2, which can be utilized by downstream units [2]. For example, NO_2 emitted from the DOC can oxidize soot trapped in the Diesel Particulate Filter (DPF). NO_2 can also be involved in the fast Selective Catalytic Reduction of NO_x ($2NH_3 + NO + NO_2 \rightarrow 2\,N_2 + 3\,H_2O$) in the SCR unit. The development of an efficient DOC needs to consider two main points, namely, the reaction conditions and the stringent requirement of modern regulation. The exhaust gas emitted from a diesel engine has a complex composition with heavy hydrocarbons, a large amount of water, some poisoning agents, and lean conditions due to a high air/fuel ratio. Moreover, the exhaust gas temperature is also lower than the gasoline counterpart. To adapt to stringent regulations under such harsh reaction conditions, the use of Platinum group metals (PGM) in the development of the DOC is indispensable. Traditional DOCs use Pt but modern DOCs are predominantly based on Pt-Pd bimetallic catalysts [3]. The addition of Pd improves the sintering resistance of Pt, although monometallic Pd is less active than its Pt counterpart for NO and hydrocarbon oxidation (except CH_4) and more susceptible to sulfur poisoning [2,3]. However, the Pd-based catalysts are generally more active than their Pt counterparts for CO oxidation [2].

Some studies have been performed to investigate the activity of Pt-Pd catalysts for DOC, including both technical papers [3–8] and research articles [9–12]. More information about the literature on Pt-Pd catalysts for DOCs published before 2011 can be found in the review by Russell and Epling [2]. The bimetallic Pt-Pd catalysts have been reported to be more active than the monometallic Pt catalysts for some reactions. For example, bimetallic Pt-Pd catalysts showed better performance than Pt catalysts for CO [4,5,10,13] and hydrocarbon oxidations [10,14,15]. For NO oxidation, bimetallic Pt-Pd usually showed lower conversion than monometallic Pt counterparts due to a lower number of Pt active sites [3,10,16–18]. Bimetallic Pt-Pd catalysts also showed better resistance to sulfur poisoning than their monometallic counterparts [16,19]. Therefore, understanding the effect of Pt/Pd ratios on the activity of the

* Corresponding authors.
E-mail addresses: phuoc@chalmers.se (P.H. Ho), louise.olsson@chalmers.se (L. Olsson).

https://doi.org/10.1016/j.jece.2022.108217
Received 21 February 2022; Received in revised form 2 June 2022; Accepted 4 July 2022
Available online 6 July 2022

bimetallic Pt-Pd catalysts is essential in the design of the DOC. Some papers have reported the effect of Pt/Pd ratios on the activity of the Pt-Pd bimetallic catalysts for a DOC [3,5,8,18,20,21]. Recently, Kang and co-workers investigated the effect of Pt-Pd ratios for Pt-Pd/Al_2O_3 catalysts on the oxidation of CO and mixed hydrocarbons (C_2H_4, C_2H_6, alkane C_6H_{14}, and aromatic C_7H_8) and stated that there was not one optimum ratio that gave the best oxidation performance for all of the multiple components in the gas mixture. The results of the experiments with simple feed might not be directly correlated to those from the experiments with a complex mixture [22]. All of the studies of bimetallic Pt-Pd have been focused on alumina supports [3,5,8,18,20,21], silica-doped alumina [15], and ceria-doped alumina [23]. The use of zeolites as supports for DOC has been rarely reported in the literature, although some patents claimed the use of ZMS-5 and beta zeolites for DOC [24,25]. Zeolites are widely studied for exhaust gas treatment systems such as passive NO_x adsorbers (PNAs) [26–28] and methane oxidation [29,30]. Zeolite Beta (BEA) and ZSM-5 have been proposed as effective supports for DOC [27]. In our previous study, we found that the use of beta zeolite as a support, in particular the one with high silica-alumina ratios, can enhance the oxidation performance of the DOC [31]. Especially, Pt/BEA was the promising catalyst in terms of the oxidation activity and sulfur regeneration, because it exhibited better performance than the benchmark Pt/Al_2O_3 and other zeolite-based catalysts (Pt/ZSM-5 and Pt/Y) for CO, NO, C_3H_6, and C_3H_8 oxidation [32].

However, to the best of our knowledge, there are no reported studies where the effect of combining Pt and Pd on highly silicious zeolites used for DOC applications is presented, which is the objective of the current study. This study investigates the effect of the Pt/Pd ratio on the physicochemical properties, oxidation activity, and sulfur poisoning resistance of the catalysts in the treatment of emissions from diesel engines. Two aspects were mainly the focus including (i) the oxidation activity for CO, NO, and hydrocarbons (C_3H_6 and C_3H_8) and (ii) the sulfur resistance and regeneration ability of the catalysts. Various characterization techniques were employed including ICP-SFMS, XRD, TEM, N_2 physisorption, CO chemisorption, XPS, CO-TPR, O_2-TPO, and DRIFTS, to correlate the structure-activity with the catalysts for the oxidation reactions as well as sulfur interaction/regeneration.

2. Experimental section

2.1. Catalyst preparation

A commercial beta zeolite (CP811C300, H^+ form) purchased from Zeolyst was used as the support for the preparation of the catalysts. The silica-alumina ratio (SiO_2/Al_2O_3) determined by elemental analysis (ICP-SFMS) was approximately 217 [32]. The zeolite was calcined at 550 °C for 6 h and denoted as H-BEA. $Pt(NO_3)_4$ (15 wt% Pt) and Pd $(NO_3)_2$ (10 wt% Pd) from Alfa Aesar were used. Five catalysts with different loadings of Pt and Pd were prepared using an incipient impregnation method. Firstly, 2 wt% Pt/BEA and 1.1 wt% Pd/BEA which have the same total molar number of Pt and Pd were prepared using the same protocol described in our previous work [32]. The catalysts were dried in air at 80 °C for 24 h and then calcined at 550 °C for 2 h with a heating rate of 5 °C min^{-1}. These two monometallic catalysts were denoted as Pt1 and Pd1, respectively. The other three catalysts contained the same total molar amount of noble metals, but with different molar ratios of Pt/Pd = 3/1, 1/1, and 1/3. These samples were prepared using a sequential impregnation step, first with Pd and then Pt as reported in the previous study [16]. The catalysts were denoted as Pt3Pd1, Pt1Pd1, and Pt1Pd3, respectively. It should be noted that between the two impregnation steps, the samples were dried and calcined under the same conditions as used for the monometallic catalysts.

Approximately 500 ± 10 mg powder of each material was coated on the honeycomb monolith (Cordierite, Ø = 21 mm, L = 20 mm) with a dip-coating method using a mixture of ethanol and water as solvent. Detailed information for the preparation of the monoliths can be found elsewhere [16].

2.2. Characterization techniques

All the as-prepared powder materials were degreened and pretreated (Section 2.3.1) before the characterization experiments. The catalysts were characterized with X-ray diffraction (XRD), N_2 physisorption, CO chemisorption, CO-TPR, O_2-TPO, X-ray photoelectron spectroscopy (XPS), and high-resolution transmission electron microscopy (HRTEM), Diffuse Reflectance Infrared Fourier Transform Spectroscopy (DRIFTS). The compositions of the as-prepared catalysts were determined with elemental analysis using inductively coupled plasma sector field mass spectrometry (ICP-SFMS). Details on the methods and the instruments for each technique can be found elsewhere [16].

XRD analysis was performed using a D8 Advance Diffractometer (Bruker AXS, Germany, Cu Kα radiation). The pattern was recorded over the 2θ range of 5–60° with a step size of 0.02° and a step time of 1 s. Cell parameter (a) was calculated using Eq. (1) for a cubic structure:

$$a = \frac{\lambda}{2sin\theta}\sqrt{h^2 + l^2 + k^2} \quad (1)$$

where λ is the X-ray wavelength (0.15406 nm for Cu Kα), θ is the Bragg angle, and h,k, and l are the Miller indices of the planes. Lattice parameters of each sample were calculated for two planes Pt(111) and Pt (200) and an average value was reported.

High-resolution transmission electron microscopy (HRTEM) images were recorded using an FEI Titan 80–300 with high-angle annular dark-field (HAADF) and energy dispersive spectroscopy (EDS). From TEM images taken at different locations, 179, 360, and 444 particles were counted for the samples Pt1, Pt1Pd1, and Pd1, respectively. The average particle sizes and distributions were processed using ImageJ software.

Temperature-programmed reduction with CO (CO-TPR) and temperature-programmed oxidation with O_2 (O_2-TPO): A sequential measurement of the 1st CO-TPR, O_2-TPO, and the 2nd CO-TPR was performed using a calorimeter (Setaram Sensys) coupled with a mass spectrometer (Hidden HR20). Approximately 30 mg of sieved catalyst (particle size of 0.18–0.25 mm) was placed in a fixed-bed quartz reactor (I.D. 4 mm). The catalyst was heated to 300 °C for 30 min (temperature ramp 5 °C min^{-1}) in Ar (20 mL min^{-1}) and then cooled to 25 °C in the same gas flow. The gas was subsequently switched to a flow of 20 mL min^{-1} of 1000 ppm CO in Ar. The temperature was subsequently ramped from 25 to 600 °C with a rate of 10 °C min^{-1} and held at 600 °C for 1 h. CO consumption was monitored by the mass number $m/z = 28$. After that, the catalyst was cooled down to 25 °C in Ar (20 mL min^{-1}). When the temperature was stable at 25 °C, a gas containing 500 ppm O_2 in Ar (20 mL min^{-1}) was introduced to the reactor. The O_2-TPO measurement was performed with increasing temperature from 25 to 500 °C (10 °C min^{-1}) and held at 500 °C for 30 min. Oxygen consumption was monitored by the mass number $m/z = 32$. After that, the catalyst was cooled down to 25 °C in Ar (20 mL min^{-1}). When the temperature was stable at 25 °C, the second CO-TPR measurement was repeated under the same condition as the first.

2.3. Catalytic tests

The activity tests were performed with a coated monolith in a flow reactor system. The flow reactor consisted of a horizontal quartz tube, which was 2.1 cm in inner diameter and 78 cm long. The temperature was controlled with a Eurotherm temperature controller and the gas and water flow were regulated with Bronkhorst® mass flow controllers and Bronkhorst® CEM system, respectively. The outlet gases were measured with a MultiGasTM 2030 FTIR from MKS.

2.3.1. Degreening and pretreatment

Before doing the activity test, the catalysts were stabilized by exposure to degreening and pretreatment steps (see Table 1).

2.3.2. Activity experiments, sulfur poisoning, and regeneration

A sequential experiment was performed for each catalyst, which resulted in 68 h of time-on-stream as described in Table 1.

The conversion of each component was calculated using Eq. (2):

$$X\ (\%) = (C_{in} - C_{out})/C_{in}*100\ (\%) \quad (2)$$

The concentration of N_2 produced from the reduction of NO with hydrocarbon was calculated based on the nitrogen mass balance using Eq. 3:

$$C_{N2} = (C_{in,\ NO} - C_{out,\ NO} - C_{out,\ NO2} - 2*C_{out,\ N2O})/2 \quad (3)$$

in which C_{in} and C_{out} are the inlet and outlet concentrations of each component.

3. Results and discussion

3.1. Characterization of the catalysts

The Pt and Pd content of the five catalysts measured by ICP-SFMS are shown in Table 2. The total noble metal contents were in a range of 99–119 μmol g^{-1}. The molar ratios of Pt:Pd were 2.5:1.0, 1.1:1.0, and 1.0:3.2, for Pt3Pd1, Pt1Pd1, and Pt1Pd3, respectively. These ratios were slightly deviated from the theoretical values due to a deviation in the assay of the noble metal precursors. The impregnation with such a low loading does not significantly alter the porosity of the catalysts. All five samples had similar specific surface areas of 598–601 $m^2\ g^{-1}$, which was only lesser than that of the H-BEA parent zeolite by about 4.5 %.

Table 1
Experiment procedure and reaction conditions.

Step	Experiment	Conditions
1	Degreening	(i) 2 % H_2 and 5 % H_2O in Ar for 30 min at 500 °C; (ii) 500 ppm NO, 8 % O_2 and 5 % H_2O in Ar for 2 h at 700 °C
2	Pretreatment	500 °C: i) 10 % O_2 and 5 % H_2O in Ar for 15 min; ii) 5% H_2O in Ar for 15 min; iii) 1 % H_2 and 5 % H_2O in Ar for 15 min; iv) 5 % H_2O in Ar for 15 min; and v) 10 % O_2 and 5 % H_2O in Ar for 15 min
3	Test T1	2 cycles from 120 to 500 °C (heating rate 10 °C min^{-1}) in a gas mixture of 500 ppm NO, 1000 ppm CO, 500 ppm C_3H_6, 500 ppm C_3H_8, 10% O_2, and 5 % H_2O in Ar
4	Pretreatment	The same as Step 2
5	Test T2	Pt1, Pt3Pd1, Pt1Pd1, and Pt1Pd3 catalysts: 250 °C for 10 h in 500 ppm NO, 10 % O_2 and 5 % H_2O in Ar Pd1 catalyst: 250, 300, 350, 400, 450 °C and 2 h for each temperature
6	Pretreatment	The same as Step 2
7	Test T3 (T-step)	7 temperature points from 150 to 450 °C (50 °C interval) and 30 min for each point in the same gas mixture as test T1
8	Reduction	At 600 °C in 2 % H_2 in Ar for 30 min
9	Test T4 (T-step)	7 temperature points from 150 to 450 °C (50 °C interval) and 30 min for each point in the same gas mixture as test T1
10	Sulfur poisoning	200 °C for 4 h in 20 ppm SO_2, 500 ppm NO, 1000 ppm CO, 500 ppm C_3H_6, 500 ppm C_3H_8, 10 % O_2 and 5 % H_2O in Ar
11	Test T5 (T-step)	7 temperature points from 150 to 450 °C (50 °C interval) and 30 min for each point in the same gas mixture as test T1
12	Regeneration R1	At 600 °C for 30 min in the same gas mixture as test T5
13	Test T6 (T-step)	7 temperature points from 150 to 450 °C (50 °C interval) and 30 min for each point in the same gas mixture as test T1
14	Regeneration R2	At 600 °C 2 % H_2 in Ar for 30 min
15	Test T7 (T-step)	7 temperature points from 150 to 450 °C (50 °C interval) and 30 min for each point in the same gas mixture as test T1

The XRD patterns of the different zeolite-supported PtPd catalysts after the degreening (at 700 °C) and a pretreatment step (500 °C) are shown in Fig. 1. The XRD pattern of the Pd1 catalyst exhibited two peaks of PdO (ICDD2020, PDF #041–007–6608) at 34.7 and 54.7°, corresponding to PdO(101) and PdO(112), respectively [10]. The first peak at 34.7° partially overlapped with the peak at around 34.4° of the zeolite support. The second peak at 54.7° almost disappeared in the patterns of the bimetallic samples which could be associated with a decrease in Pd loading or a transformation of PdO into PdPt alloy in the bimetallic samples. The pattern of Pt1 catalyst had two intense peaks related to Pt (ICDD2020, PDF #01–070–2057), apart from the reflections of the zeolite support (Fig. 1). These peaks were at approximately 39.7 and 46.1° which refer to the reflections of Pt(111) and Pt(200), respectively. It is noted that these peaks were shifted to higher diffraction angles in the cases of bimetallic PtPd samples, and the shifts increased with the increment of the Pd amount (Fig. 1b). This trend agrees with those reported in the literature [33]. We note that the diffractions of the zeolite support were not shifted as the diffractions of Pt were. Therefore, the shifts of the reflections of Pt suggest the formation of the PtPd alloys on the bimetallic samples, leading to a reconstruction of the Pt structure [14]. To verify this point, we calculated the cell parameters for a cubic structure of Pt for the two planes Pt(111) and Pt(200), and the average values of cell parameters are plotted in Fig. 1d. The Pt1 sample had a lattice constant of 3.927 Å which was similar to the one reported in the literature [34]. The values of lattice constants decreased steadily with an increase in the Pd loading, e.g. the value was 3.903 Å for the Pt1Pd3 catalyst. Both metallic Pt and Pd have the same phase of face-centered cubic (fcc) but Pd has a smaller lattice constant (3.89 Å) than that of Pt (3.92 Å) [34]. The small lattice mismatch between Pt and Pd, therefore, accounted for a contraction of the lattice constants of the bimetallic PtPd samples.

The TEM images and particle size distributions are shown in Fig. 2, while the average sizes of the particles are summarized in Table 2. Several images were used to determine the particle size distribution and 179, 360, and 444 particles were counted for Pt1, Pt1Pd1, and Pd1, respectively. The Pd1 catalyst had an average particle size of approximately 12.4 ± 5.3 nm (Fig. 2f) which was slightly smaller than that of the monometallic Pt1 sample (15.4 ± 4.3 nm, Fig. 2b), which is consistent with our previous study with Pt and Pd supported on Al_2O_3 [16]. This is due to better resistance for sintering of Pd than Pt during the high-temperature degreening (700 °C). Bimetallic catalysts, e.g. Pt1Pd1, had an average size of the particles of approximately 14.0 ± 7.8 nm which was in between the Pd1 and Pt1 samples. HRTEM with EDS mapping was conducted and the results of the elemental mapping of the Pt1Pd1 sample are shown in Fig. 3. Inspecting the Pd and Pt particles in the EDS mapping shows a clear overlap, indicating the formation of a PtPd alloy, which is consistent with the XRD results (Fig. 1). In the literature, the formation of such PtPd alloys improved the sintering resistance of Pt with the addition of Pd on the alumina support [16,33,35], which agrees with our findings.

CO chemisorption experiments were performed to obtain further information about the particle sizes of the catalysts. Table 2 shows the amounts of CO adsorbed and the average noble metal particle size. The particle size was increasing in the order Pt1Pd3 (6.8 nm) < Pd1 (10.4 nm) < Pt3Pd1 (11.1 nm) ≈ Pt1Pd1 (11.6 nm) < Pt1 (15.6 nm). This confirms the improvement of the sintering resistance of Pt with the addition of Pd, as also was observed with TEM (Fig. 2).

The oxidation states of Pt and Pd species play an important role in the activity of the DOC catalysts and XPS measurements were therefore performed. Fig. 4 displays the XPS spectra of the Pt4f and Pd3d core levels of the catalysts. Detailed information on the binding energy and the amount of each oxidation state are summarized in Table 3. The Pt1 catalyst shows the peak position of Pt4f7/2 at 71.9 eV which was similar

Table 2
Physicochemical properties of the catalysts.

Catalyst	Pt[a] / wt%	Pd[a] / wt%	Pt:Pd molar ratio	S_{BET} / $m^2\ g^{-1}$	$S_{external}$ / $m^2\ g^{-1}$	V_{pore} / $cm^3\ g^{-1}$	TEM particle size / nm	CO[b] / μmol g^{-1}	CO/ (Pt+Pd)[b] / molar ratio	Particle size[b] / nm
Pt1[c]	2.24	–	1:0	598	171	0.33	15.4 ± 4.4	8.0 ± 0.3	0.070	15.6
Pt3Pd1	1.66	0.36	2.5:1	600	172	0.33	–	9.5 ± 0.2	0.080	11.1
Pt1Pd1	1.14	0.57	1.1:1	601	173	0.34	14.0 ± 7.8	7.4 ± 0.5	0.066	11.6
Pt1Pd3	0.46	0.80	1:3.2	601	170	0.33	–	9.4 ± 0.2	0.095	6.8
Pd1	–	1.18	0:1	600	170	0.34	12.4 ± 5.3	6.0 ± 0.5	0.054	10.4
H-BEA	–	–	–	628	168	0.34	–	–	–	–

[a] Determined with ICP-SFMS.
[b] Determined with CO chemisorption measurements and the size for a spherical particle.
[c] Data was cited from our previous work [32].

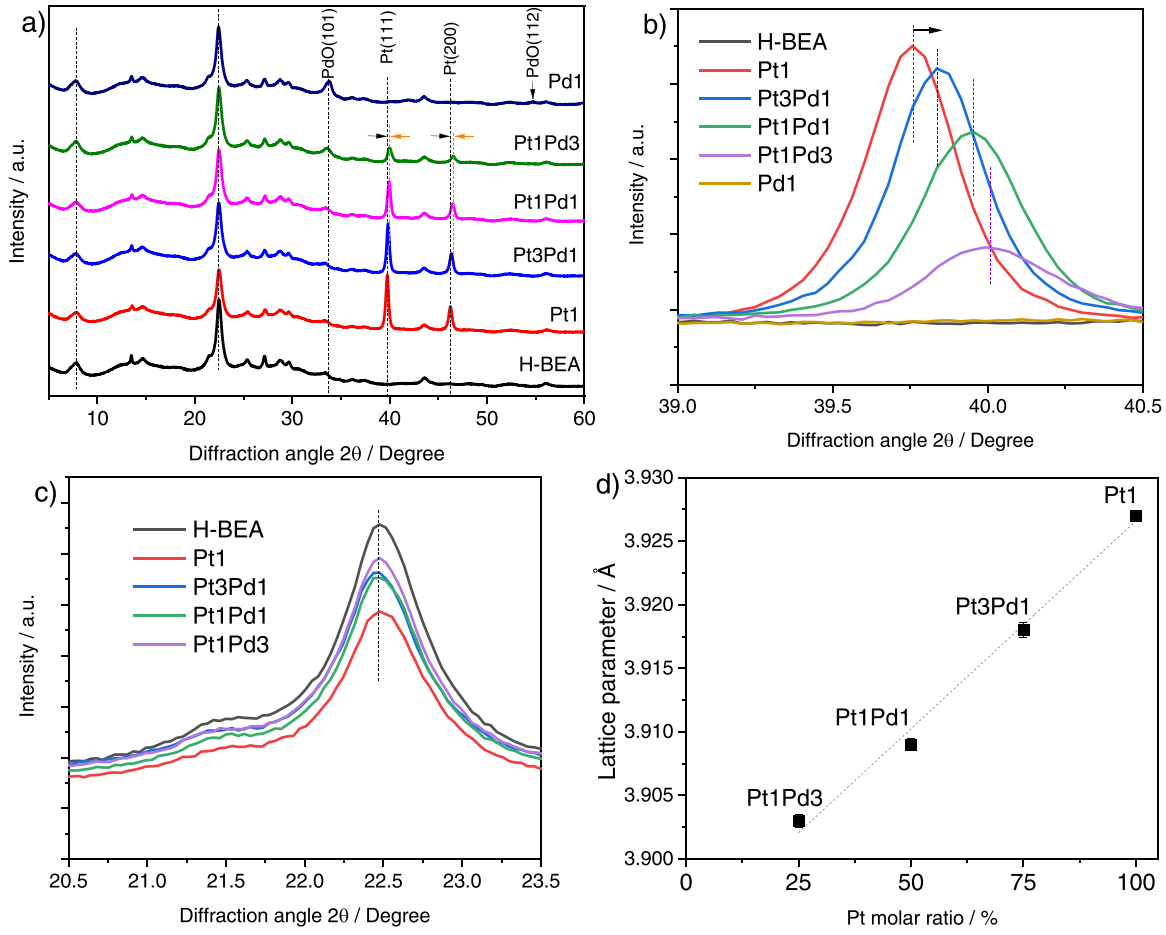

Fig. 1. a) XRD patterns of H-BEA zeolite support and Pt-Pd/BEA catalysts with different Pt/Pd ratios; b) The enlargements of the Pt(111) reflection; c) The enlargements of the main reflection of beta zeolite, and d) Relationship between the amount of Pt (%) and the lattice parameter (Å).

to that of Pt4f7/2 reported in the literature for zeolite-supported Pt [36, 37], or silica-supported Pt catalysts [38]. The Pt1Pd3 sample had the same BE of Pt4f7/2 as the Pt1, while the Pt3Pd1 and Pt1Pd3 exhibited lower BEs, at 71.5 and 71.7 eV, respectively. The major part of the Pt has oxidation states between 0 (71.0 eV) and + 2 (72.5 eV) [38]. In addition, the presence of some Pt^{+4} which usually shows binding energy at approximately 74.5 – 74.9 eV [39] could be identified. However, it should be noted that the overlap between the binding energy of the Pt4f and Al2p core levels [40,41] makes the analysis difficult. A careful analysis of Pt4f core level for each sample was performed with a consideration of the overlap between the binding energy of Al2p and Pt4f [40]. An estimation of the fraction of each oxidation state are reported in Table 3. In the monometallic Pt1 sample, Pt^{+2} was the dominant oxidation state (83.3 %) while Pt^0 and Pt^{+4} were lesser than 10 % for each fraction. In the bimetallic catalysts, the oxidation state of Pt was strongly influenced by the loading of Pd. The relationship between the fraction of Pt^0 and Pd loading exhibited a volcano relationship with a maximum of Pt^0 fraction around 38.5 % in the Pt3Pd1 sample (25 % Pd). The fraction of Pt^{+2} and Pt^{+4} mostly followed a reverse trend with the Pt^0. It is also noted that for XPS measurements using a monochromatic Al Kα source (1486.6 eV) only the surface layer of zeolite, determined by the electron mean free path (EMFP) of approximately 4 nm, contributed to the XPS signal [41]. Consequently, the XPS data confirmed the presence of Pt oxides only a few nanometers from the surface of the catalyst. This could be the reason that no oxide phase was detected by XRD in which the signal represented an average of the entire sample. Moreover, XRD cannot detect small particles (e.g. <2 nm) [15], and it is known that large Pt particles are more difficult to be oxidized.

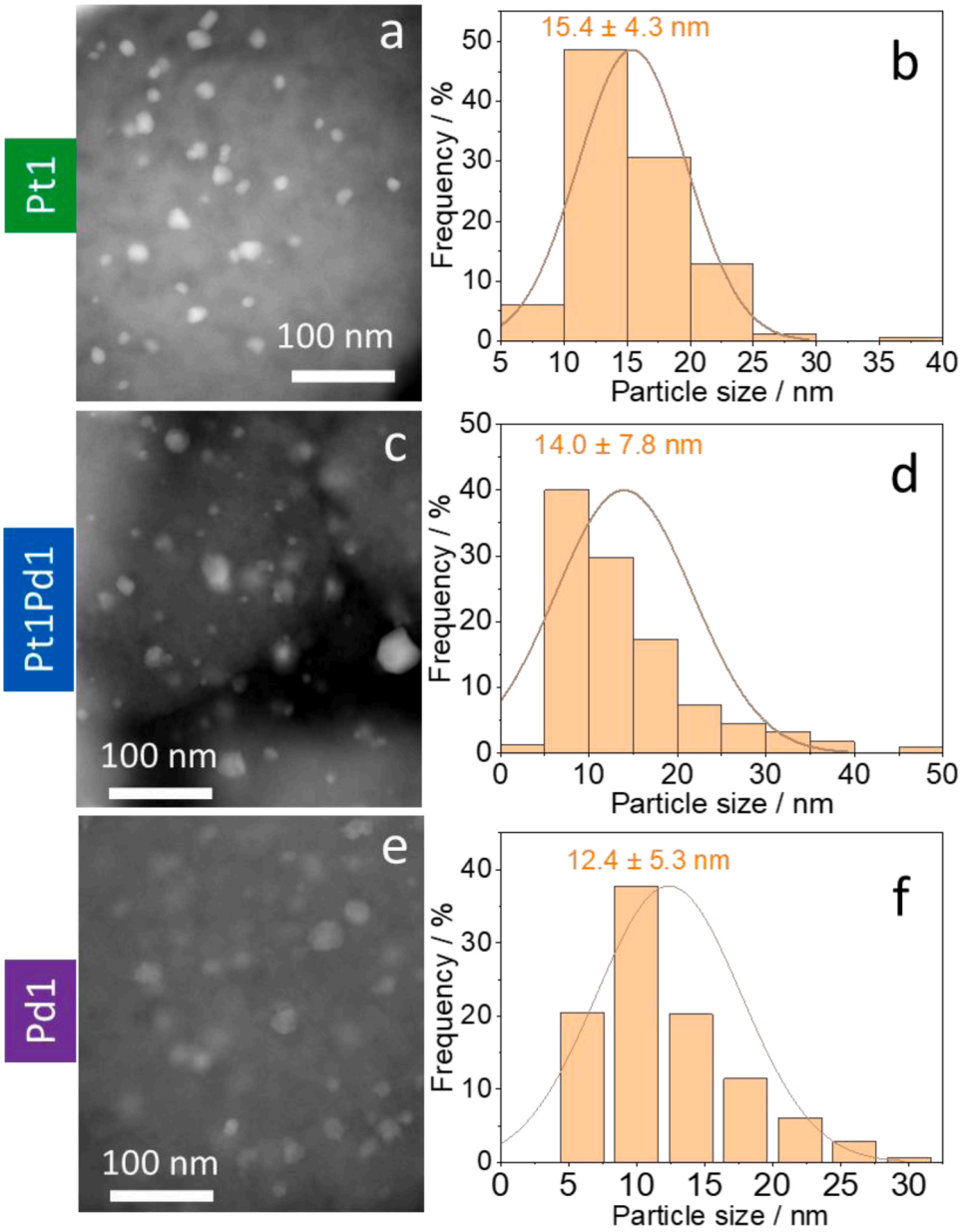

Fig. 2. TEM micrographs (a, c, e) and particle distributions (b, d, f) of Pt1, Pt1Pd1, and Pd1 catalysts. Data for the Pt1 sample (Fig. 1b) was reproduced from reference [32].

Therefore, it is not surprising the XRD showed only a metallic phase [40].

By contrast to the Pt1, only Pd^{+4} surface species were found on the Pd1 sample with a peak around 337.5 eV [39]. Higher resistance for oxide formation on Pt than Pd can explain the presence of some metallic Pt in the Pt1, but only Pd^{+4} in the Pd1 sample. In bimetallic samples, the peaks of Pd*3d* were slightly shifted to lower binding energies. These peaks were deconvoluted into two peaks at approximately 337.5 and 335.8 eV, which were assigned to Pd^{+4} and Pd^{+2}, respectively [39]. The loadings of Pt influenced the oxidation state of Pd species in the bimetallic catalysts. A higher ratio of Pt induced the formation of a higher fraction of Pd^{+2} than the Pd^{+4}. For example, the bimetallic Pt1Pd3 sample (25 % mole of Pt) had a fraction of Pd^{+4} of approximately 88 % (Table 3). When increasing the Pt ratio to 75 % in the sample Pt3Pd1, the Pd^{+4} fraction dropped to 20 %. In summary, the XPS data suggested that the addition of Pd into Pt could inhibit the further oxidation of the surface species of both Pt and Pd, e.g. decreasing the fraction of surface Pt^{+4} and Pd^{+4} species due to the formation of PtPd alloy as evidenced by XRD.

Sequential measurements of CO-TPR, O_2-TPO, and CO-TPR were performed to investigate the reduction and oxidation properties of the catalysts (Fig. 5). The first CO-TPR profile of the Pd1 had three peaks (Fig. 5a). The first one was a positive weak peak at around 65 °C due to the desorption of the weakly adsorbed CO molecules. This peak was observed for all samples, even in the second CO-TPR cycle (Fig. 5c). Two negative peaks at approximately 256 °C and 600 °C (isothermal zone) were observed and we assigned them to the consumption of CO by the reduction of small and large particles of PdO, respectively. This assignment is consistent with the assignment by Luo et al. [42], who studied Pd/CeO_2, although their CO reduction occurred at lower temperatures compared to our results.

After the first CO-TPR cycle, the catalyst was purged with Ar, cooled to 25 °C, and the O_2-TPD was thereafter performed. The O_2-TPD profile of the Pd1 exhibited two negative peaks, one weak peak at 85 °C and another strong peak at 365 °C due to the re-oxidation of the metallic Pd formed during the first CO-TPR cycle. The second CO-TPR profile for

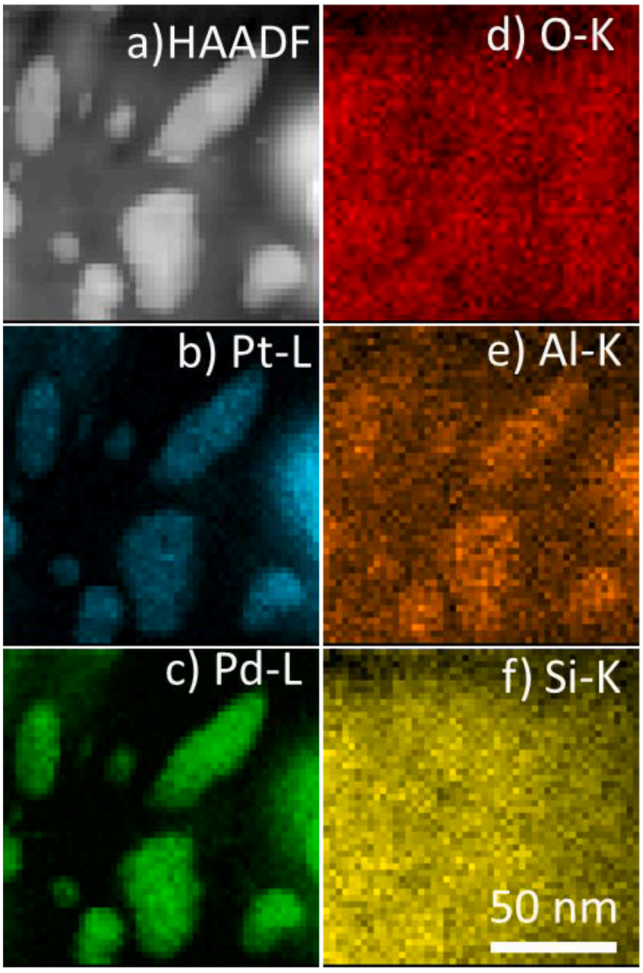

Fig. 3. Elemental mappings of the Pt1Pd1 catalyst.

Pd1 (Fig. 5c) had a similar shape as the first CO-TPR, except that the third peak at 600 °C almost disappeared. The disappearance of the high-temperature peak indicated that there were almost no large PdO particles after the first cycle of CO-TPR and O_2-TPD. This could be explained by the redispersion of Pd species during the reduction with CO and re-oxidation with O_2 during the first CO-TPR and O_2-TPD, respectively, as reported in the literature [43].

The reduction-oxidation behavior of Pt is different from Pd. The first CO-TPR profile of the Pt1 catalyst showed one peak of CO consumption at 600 °C (Fig. 5a). This peak was similar to the high-temperature peak of the Pd1 catalyst and was assigned to the reduction of PtO particles. Pt has better oxidation resistance than Pd and it is hardly oxidized in O_2 up to 500 °C [44]. Indeed, the O_2-TPD profile showed almost a flat curve from 100 °C to 500 °C, indicating no consumption of O_2 up to 500 °C (Fig. 5b). A small peak at around 95 °C was likely due to the chemisorption of O_2 on the Pt particles (Fig. 5b). Since Pt was barely oxidized during the O_2-TPD, no consumption of CO was observed in the second CO-TPR experiment (Fig. 5c).

All three bimetallic PtPd samples had similar profiles for CO-TPR and O_2-TPD, suggesting that they had similar properties in the reduction-oxidation. Moreover, the CO-TPR and O_2-TPD profiles for these bimetallic samples are similar to those of the Pt1 rather than the Pd1. For example, the O_2-TPD profiles showed a flat profile without a peak at around 365 °C while the second CO-TPR profile displayed only a negligible peak at around 600 °C. This indicated that the metallic particles in the bimetallic samples were more difficult to oxidize during the O_2-TPO. Therefore, it can be concluded that in the bimetallic samples the formation of PtPd alloy inhibited the reoxidation of PtPd particles and subsequently retained these particles in a high fraction of the metallic form.

DRIFTS measurements using CO as a probe molecule were performed to investigate the characteristics of the Pt and Pd species. Fig. 6 presents the spectra of adsorbed CO on monometallic and bimetallic Pt-Pd/BEA catalysts. Pt/BEA catalyst had two distinct bands, a sharp strong band at 2098 cm^{-1} and a broad weak band at 1945 cm^{-1}. The former can be assigned to linear-bonded CO on large Pt particles [45]. The latter was attributed to either the carbonyl complex $Pt_3(CO)_6^{2-}$ [46] or the adsorption of CO in the bridged coordination [47]. Similar bands as those at 2098 and 1945 cm^{-1} were also observed on Pd/BEA and could be interpreted similarly. In addition, the spectrum of the Pd/BEA sample showed four other bands at 2153, 2135, 2118, and 2077 cm^{-1}. The band at 2077 cm^{-1} was assigned to linear CO adsorbed on metallic Pd (Pd^0-CO) like the band at 2098 cm^{-1}, and the slight shift could be due to different particle sizes [48,49]. The bands at 2135 and 2118 cm^{-1} were assigned to CO adsorbed on Pd^{2+} and Pd^{+} [43,50]. The spectra of adsorbed CO on the bimetallic Pt-Pd samples not only included the superpositions of the two corresponding monometallic Pt and Pd samples but also had some other characteristic features. For example, the peak around 2135 cm^{-1} slightly decreased in intensity and a new shoulder appeared at 2125 cm^{-1} in the Pt3Pd1 sample. This indicated a decrease in the amount of CO adsorbed as Pd^{2+}-CO and an increase in the number of Pd^{+}-CO. Thus, the result well agreed with the XRD data, where more Pd species existed in the reduced form due to the formation of the Pt-Pd alloy.

3.2. Activity measurements

3.2.1. Cycle tests

Fig. 7 presents the conversions of CO, NO, C_3H_8, and C_3H_6 on the catalysts with different ratios of Pt/Pd during two consecutive cycles. The temperatures at which 50 % of CO, C_3H_8, and C_3H_6 were converted on each catalyst, T_{50}, are summarized in Table 4 and also shown in Fig. 8.

3.2.1.1. CO oxidation. For the monometallic catalysts, Pd1 was less active for CO oxidation than Pt1 in the first cycle test, with temperatures for 50 % conversion (T_{50}) of 248 and 171 °C, respectively. The CO conversion profile for Pt1 was shifted to a higher temperature in the second cycle whereas a reverse trend was observed on the Pd1 sample (Fig. 7a). As a result, the difference in T_{50} between the second and the first cycle test was +44 and −43 °C for the Pt1 and the Pd1 catalyst, respectively. These trends for the CO conversion profiles were similar to those for the same types of catalysts (Pt/BEA and Pd/BEA) prepared by a wet impregnation route reported in our previous work [31]. In the second cycle, the Pd1 catalyst had a T_{50} of 205 °C, which was lower than the T_{50} for the Pt1 catalyst (215 °C). However, the Pd1 catalyst reached a full conversion of CO at around 260 °C which was approximately 15 °C higher than that of the Pt1 catalyst (full CO conversion at 245 °C). These results suggest that Pt1 was more active than the Pd1 catalyst for CO oxidation under the reaction conditions in this study. Furthermore, in our previous work, we found that the T_{50} of the second cycle was 206 and 245 °C for the Pd1 and Pt1, respectively, which were prepared by wet impregnation instead of incipient impregnation [32]. Both samples of the Pd1 had similar T_{50} values regardless of the preparation method whereas the Pt1 prepared with the incipient impregnation showed a substantially lower T_{50} value than the one prepared by wet impregnation. This indicates that the preparation method was more sensitive for Pt than Pd supported on zeolites.

Dubbe et al. [51] have observed a decrease in CO conversion between two cycles for a Pt/Pd DOC and suggested that this could be related to three main factors including a change in the oxidation state of the nobles metals, CO self-poisoning, and the interference by C_3H_6. We also observe a decrease in the CO conversion between the first and the

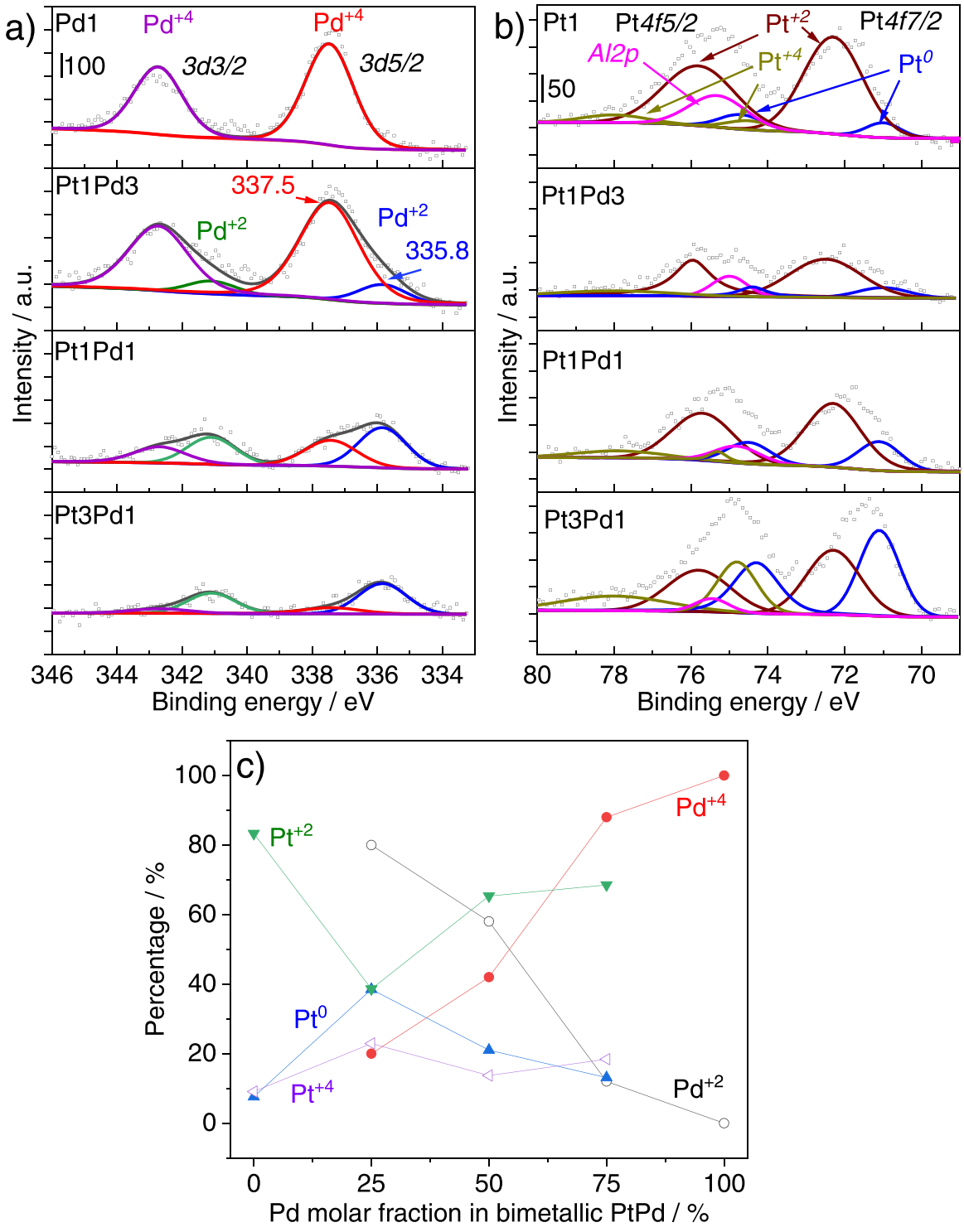

Fig. 4. The XPS spectra for a) Pd and b) Pt species, and c) the relationship between the fraction of noble metal species on the surface versus the Pd loading in the Pt-Pd samples. The scattered symbols in (a) and (b) indicate the original data. Note that the y-xis of every layer in each graph (a and b) was plotted with the same scale.

second cycle for the monometallic Pt1 and we hypothesize that after the pre-treatment the Pt sites of the Pt1 catalyst are fresh and free and therefore CO oxidation can occur at low temperature in the first cycle. However, during the first cycle, the conversion of C_3H_6 might produce different adsorbed hydrocarbon species on the catalyst surface and partially block the available sites for CO. This could explain the inflection observed in the first cycle. During the cooling step in the reaction mixture after the first cycle, the hydrocarbon species left on the surface of the catalyst suppressed the CO conversion. As a result, the low-temperature activity of CO oxidation is no longer visible, which was accompanied by the disappearance of the inflection. Moreover, it is also possible that the Pt sites might be partially oxidized during the first cycle, and this might also be a reason for the lower CO conversion in the second cycle.

For the Pd1 catalyst, the second cycle exhibited better CO conversion than the first cycle. This trend is contrasting with the CO conversion on both the Pt1 and Pd/Al_2O_3 under the same reaction conditions [16]. However, we noted that this phenomenon was observed for the three

Table 3
Binding energy of Pt4f7/2 and The fraction of oxidation states for Pt and Pd on the surface of different Pt and Pd supported catalysts.

Catalyst	Pt4f7/2 / eV	Pt^{+4} / %	Pt^{+2} / %	Pt^{0} / %	Pd^{+4} / %	Pd^{+2} / %
Pt1	71.9	14.4	75	13.6	–	–
Pt3Pd1	71.5	19.3	44.5	36.2	20	80
Pt1Pd1	71.7	17.4	58.1	24.5	42	58
Pt1Pd3	71.9	25.5	59.5	15.0	88	12
Pd1		–	–	–	100	0

Pd/BEA catalysts with different SiO_2/Al_2O_3 ratios (41, 217, and 501) [31]. Furthermore, the difference in CO conversion only occurred between the first can the second cycle while almost no difference in CO conversion was observed for all cycles from second to fifth [16,31]. Notably, the light-off temperatures of CO, NO, and C_3H_6 were quite close to each other in the first cycle but not for the second cycle (Fig. 7a). After the degreening and pretreatment step, the Pd might be in a high oxidation state, e.g. PdO_2 as identified by XPS, which is not very active for the oxidation of CO, explaining a high light-off temperature of CO in the first cycle. This is supported by the fact that the reduced Pd1 catalyst exhibited a higher conversion of CO than the original one (see Section 3.2.3). After the first cycle, it is possible that the Pd oxide with a high oxidation state, e.g. PdO_2, was reduced by CO (1000 ppm) during the cooling step from 500 to 120 °C under the gas mixture. Reduction of Pd in Pd/SSZ-13 during exposure to CO has previously been observed in passive NO_x adsorption experiments [52]. The Pd species with a more reduced state are more active and subsequently favored CO oxidation at low temperatures in the next cycle.

All three samples containing bimetallic PtPd were more active for CO oxidation than the monometallic samples. The T_{50} values of the catalysts in the second cycle were Pt3Pd1 = Pt1Pd1 (172 °C) < Pt1Pd3 (182 °C) < Pd1 (205 °C) < Pt1 (215 °C). All three bimetallic samples had significantly lower T_{50} values than those of the monometallic samples, indicating the advantage of the bimetallic formulation for the DOC catalysts. The alloy of Pt-Pd in the bimetallic catalysts retained the metallic Pt particles and reduced Pd-PdO_x species (Table 2), and this could explain the significant improvement in the CO oxidation compared to the monometallic catalysts. Although the trend is in line with the literature for Pt and Pd supported on Al_2O_3, the optimum Pt/Pd ratio is different. It has been reported for the alumina-based catalysts that a lower Pt/Pd ratio had a lower T_{50} value, because Pd was more active than Pt for CO oxidation [18,53,54]. In the present work, we have found that the samples with a higher Pt/Pd ratio showed a better performance for CO oxidation. This could be related to the difference between the supports of the catalysts, namely, the high SAR zeolite in the

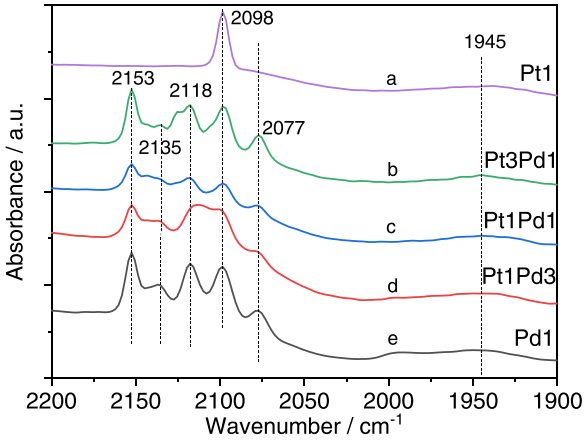

Fig. 6. DRIFT spectra of adsorbed CO species on monometallic and bimetallic Pt-Pd/BEA catalysts.

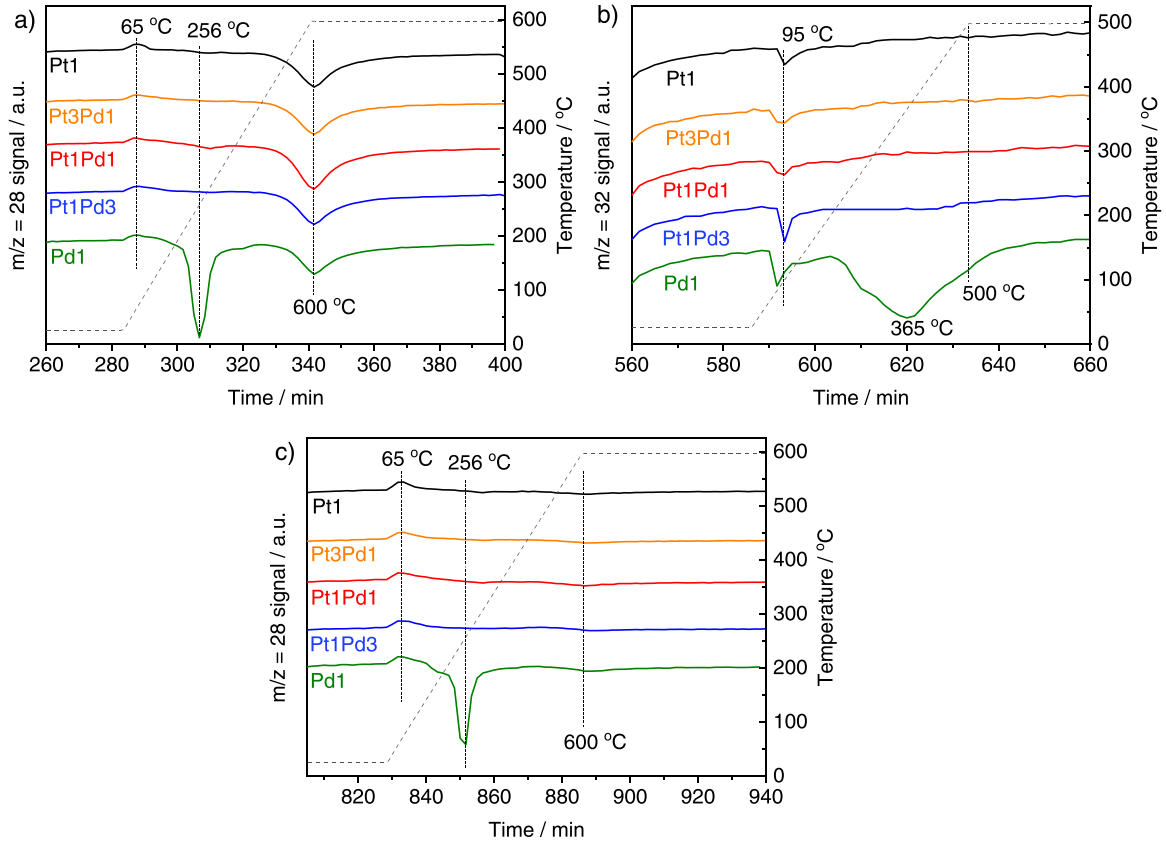

Fig. 5. a) The first CO-TPR, b) O_2-TPO, and c) The second CO-TPR profiles of different catalysts.

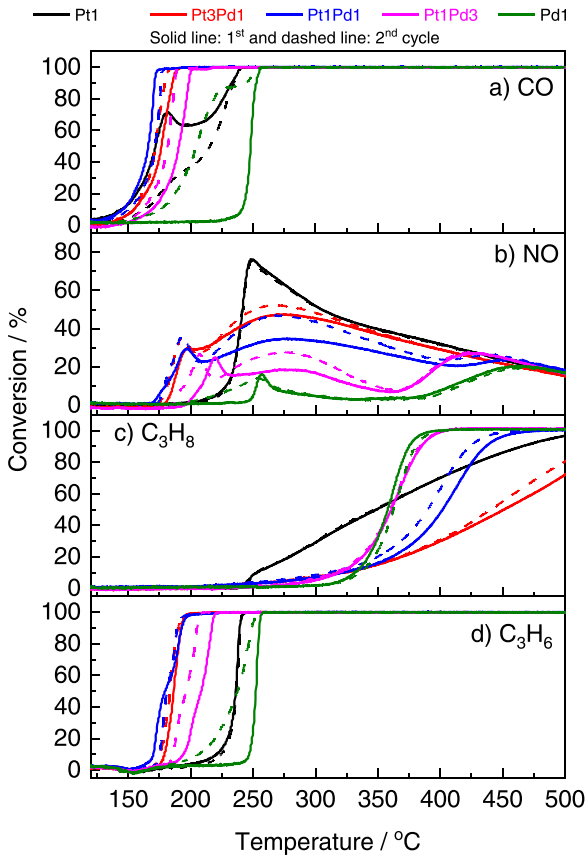

Fig. 7. Effect of Pt/Pd ratios on the conversion of CO, C_3H_6, NO, and C_3H_8 on Pt-Pd/BEA catalysts. Reaction conditions: GHSV = 22,520 h^{-1} with a total flow of 2600 mL min^{-1} of CO (1000 ppm), NO (500 ppm), C_3H_6 (500 ppm), C_3H_8 (500 ppm), O_2 (10 %), and H_2O (5 %) balanced in Ar.

Table 4
T_{50} (°C) of CO, NO, C_3H_8, and C_3H_6 for different catalysts.

Gas	Cycle	Pt1	Pt3Pd1	Pt1Pd1	Pt1Pd3	Pd1
CO	1st	171	177	166	191	248
	2nd	215	172	172	182	205
NO	1st	241	–	–	–	–
	2nd	241	–	–	–	–
C_3H_8	1st	350	452	402	361	358
	2nd	350	441	390	360	363
C_3H_6	1st	236	187	180	209	252
	2nd	236	183	181	197	238

present work and the alumina in the literature. However, the influence of the reaction conditions could not be discarded, e.g. the water contents. For example, beta zeolites with high SAR are more hydrophobic than alumina and hence the catalyst using the zeolite as support could be less sensitive to water than those using the alumina.

3.2.1.2. NO oxidation/reduction. The conversion profiles for NO on the Pt1 catalyst were almost identical between the two cycles, suggesting a stable conversion of NO. The Pt1 catalyst showed a maximum NO conversion of 76 % at 250 °C and T_{50} at 241 °C. Whereas the Pd1 catalyst was substantially less active than Pt1 with the maximum conversion of NO at approximately 16 % at 255 °C. Both Pt1 and the Pd1 catalysts in this study were more active than the Pt/Al_2O_3 and Pd/Al_2O_3 catalysts under identical reaction conditions as reported in our previous work [16]. For example, the Pt/Al_2O_3 reached the maximum conversion of NO at 60 % at 160 °C while the Pd/Al_2O_3 showed a conversion lower than 10 % at around 160 °C.

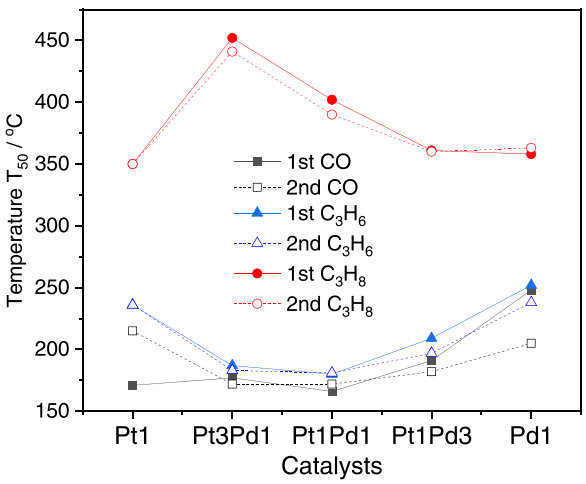

Fig. 8. Temperature for 50 % conversion (T_{50}) for CO, C_3H_6, and C_3H_8 for the catalysts with different Pt/Pd ratios.

The bimetallic catalysts exhibited maximum conversions of NO in the second cycle with an increasing order according to Pt1Pd3 (27 %) < Pt1Pd1 (46 %) < Pt3Pd1 (52 %) < Pt1 (76 %). In the literature, Pt is known to be more active than Pd for the oxidation of NO [2]. Therefore, the increase in the ratio of Pd in the bimetallic formulation led to a decrease in the maximum conversion of NO likely due to a lower number of Pt active sites. It should be noted that the NO conversion profiles of the bimetallic catalysts had a second peak at low temperatures unlike the Pt1 (Fig. S1a); however, these peaks coincided with the maximum concentration of N_2O formation (Fig. S1b). Detailed information on the concentration profiles of NO, NO_2, N_2O, and N_2 is given in Fig. S2. The data suggests that on the bimetallic catalysts, NO was reduced to both N_2O and N_2 by hydrocarbons at low temperature but it was oxidized to NO_2 by oxygen at high temperature. It was also noted that the bimetallic catalysts with high loading of Pt (Pt3Pd1 and Pt1Pd1) were more active for the NO reduction reaction. These catalysts not only facilitated the formation of N_2O at lower temperatures but also produced a slightly higher amount of N_2O than the monometallic Pt1 catalysts. The reduction of NO to N_2O by hydrocarbons, i.e. HC SCR, at low temperatures has been reported in the literature [55–57].

3.2.1.3. C_3H_6 oxidation. The trend in the activity of C_3H_6 oxidation was similar to CO oxidation. In the first cycle, the T_{50} values were 236 and 252 °C for the Pt1 and Pd1, respectively. This trend was expected since Pt is generally more active than Pd for alkene oxidation [21]. In the second cycle, both catalysts showed similar T_{50} around 236–238 °C (Table 4). However, Pt1 showed full conversion of C_3H_6 at approximately 245 °C whereas the Pd1 reached 100 % conversion at 260 °C. All three bimetallic PtPd samples were more active than the monometallic Pt1 and Pd1 for C_3H_6 oxidation. The T_{50} values of the catalysts in the second cycle were in an increasing order Pt1Pd1 (181 °C) ≈ Pt3Pd1 (183 °C) < Pt1Pd3 (197 °C) < Pt1 (236 °C) ≈ Pd1 (238 °C). For all catalysts, the conversion of C_3H_6 increased significantly when the CO conversion almost reached a full conversion due to the strong competitive adsorption of CO with C_3H_6 on the active sites. Moreover, the temperature at which C_3H_6 reached full conversion almost coincided with the N_2O peak (Fig. S1b), which could be related to the reduction of NO with C_3H_6. The best performance for C_3H_6 oxidation was found for Pt1Pd1 catalyst, which was consistent with the results reported by Hazlett et al. for the oxidation of single component C_3H_6 or a mixture of C_3H_6 and CO in an ideal condition (1500 ppm C_3H_6 (and 3000 ppm CO), 8 % O_2, and N_2 balance) using Pt and Pd supported on alumina [13]. However, other trends have also been shown in the literature, for example, that a high Pt content was optimum in the presence of water in a simulated exhaust gas [3,8,18].

3.2.1.4. C_3H_8 oxidation. C_3H_8 was more difficult to be oxidized than CO, NO, and C_3H_6 (Fig. 7). The oxidation of C_3H_8 on the Pt1 catalyst commenced instantly after the oxidation of CO, C_3H_6, and NO reached maximum conversions. The Pt1 catalyst had a T_{50} value for C_3H_8 oxidation of around 350 °C and reached approximately 98 % conversion at 500 °C. Whereas the oxidation of C_3H_8 on the Pd1 catalyst started at a substantially higher temperature than the Pt1, with T_{50} at around 363 °C, and Pd1 reached full conversion much more rapidly (at 405 °C for the second cycle). In the literature, Pt has been reported to be more active than Pd for C_3H_8 oxidation at low temperatures [58]. The Pt1Pd3 catalyst showed very similar activity to Pd1, whereas the Pt3Pd1 catalyst exhibited lower conversion than the Pt1. The Pt3Pd1 catalyst had a T_{50} of 440 °C and only reached 81 % conversion at 500 °C in the second cycle test. The Pt1Pd1 exhibited conversion between the two samples Pt3Pd1 and Pt1Pd3. The effect of Pt/Pd ratio on the oxidation of hydrocarbons has been reported for Al_2O_3 supported catalysts [3,8,18,22], but there is a lack of information for C_3H_8 in the literature. Kim and coworkers [11] have recently reported that the bimetallic Pt-Pd/Al_2O_3 (Pt/Pd = 1/1 molar ratio) catalyst exhibited slightly better oxidation conversion for C_3H_8 than the monometallic Pd; however, the presence of 0.3 % of H_2 in the gas mixture (1500 ppm of C_3H_8, iso-C_5H_{12}, and C_3H_6, 1 % CO, 500 ppm NO, 10 % O_2, and 10 % H_2O) made it difficult to compare with the present study. Moreover, there are according to our knowledge no studies in the literature that have examined the effect of the Pd/Pt ratio on high SAR zeolites used for DOC reactions, which has been reported in the current work.

3.2.2. NO stability test

NO stability tests were performed at 250 °C for 10 h and the results are shown in Fig. 9a. It should be noted that the tests were performed in the absence of CO and hydrocarbons to discard the interference of these components on NO conversion and thus NO was only oxidized without the reduction by CO/hydrocarbons. The Pd1 catalyst was almost inactive for NO oxidation at 250 °C and the NO oxidation was therefore investigated from 250 to 450 °C for this sample. But the Pd1 catalyst exhibited low NO oxidation also at higher temperatures, e.g. only about 9 % NO conversion at 400 °C. The Pt1 was the most active catalyst among the five tested. The maximum NO conversion for this catalyst was approximately 43 % and it was stable with time-on-stream. For the bimetallic catalysts, the NO conversions only declined during the first 3 – 4 h and then stabilized for the rest of the experiment. At the end of the stability test, the conversion of NO was ranked in the order of Pt1Pd3 (20 %) < Pt1Pd1 (29 %) < Pt3Pd1 (33 %) < Pt1 (43 %) (Fig. 9a).

The NO conversion is plotted versus the molar ratio of Pt/(Pt+Pd) and the results are shown in Fig. 9b. It was observed that the NO conversion increased linearly with the molar ratio of Pt/(Pt+Pd). This trend was consistent with the NO oxidation activity of the monometallic catalysts since Pt1 exhibited a significant activity while the Pd1 catalyst was inactive for NO oxidation at 250 °C. However, it was interesting to note that after 10 h of time on stream the NO conversion for the Pt1 and Pt1Pd1 was about 43 % and 29 %, respectively. This meant that the NO conversion for the Pt1Pd1 was about 30 % lower than that of the Pt1 catalyst, although the Pt loading of the former was only half of the latter. This suggests that the inclusion of Pd had a synergetic effect on the stability of the catalyst, likely related to the formation of the PtPd alloy (Section 3.1). The formation of the PtPd alloy created a larger fractions of Pd and Pt species with a lower oxidation state as seen by the XPS results (Fig. 4 and Table 3). Reduced Pt is more active for NO oxidation [40]. The Pd species were oxidized easier than the Pt species, which was observed from the O_2-TPO profile, where the Pd species were reoxidized from around 230 °C (Fig. 5b). The fast reoxidation of the Pd species might account for the fast decline in the NO conversion over the bimetallic catalysts during the first period of the stability test. Furthermore, the formation of the PtPd alloy enhanced the oxidation resistance of the Pd and Pt species and the effect was more pronounced for the sample with high fractions of Pt. As a result, the samples with a higher fraction of Pt were deactivated more slowly over a longer time and subsequently exhibited better NO oxidation activity.

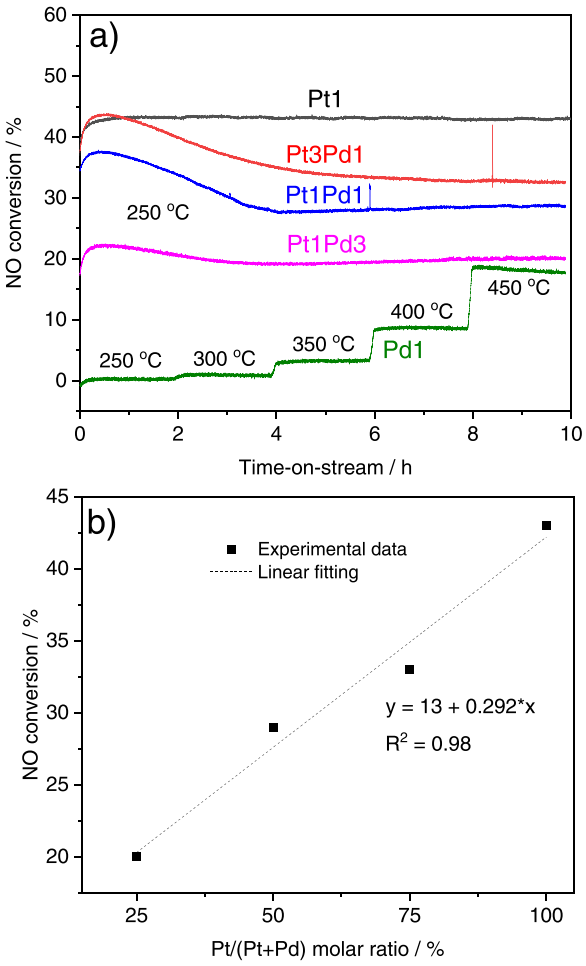

Fig. 9. a) NO conversion for different catalysts for 10 h of time-on-stream and b) the relationship between the NO conversion at the end of the stability test and the molar ratio of Pt in the bimetallic PtPd catalysts. Gas composition NO (500 ppm), O_2 (10 %), and H_2O (5 %) balanced in Ar. The temperature was 250 °C for Pt-containing catalysts and from 250 to 450 °C for the Pd1 catalyst.

3.2.3. Effect of H_2 treatment

The catalyst was pretreated after the NO oxidation stability test and subsequently tested at different temperatures from 150 to 450 °C (50 °C intervals and 30 min each step) in the complex gas mixture. After the first T-step test, the catalyst was reduced with 2 % H_2 in Ar at 600 °C and the second T-step test was repeated to study the effect of H_2 pretreatment. The conversions over the whole range of temperatures are displayed in Fig. 10. The reduction with H_2 influenced the conversion differently, depending on both the gas component and the catalyst. In general, the reduction pretreatment increased the activity of the Pd-based catalysts significantly more than the Pt ones. For example, after the reduction with H_2, the Pd1 catalyst increased the conversions for all four gases, i.e. CO, NO, and C_3H_6 at 200 °C and C_3H_8 at 350 °C (compare the solid dark cyan line (Fig. 10a) and the dashed dark cyan line (Fig. 10b)), indicating an improvement of the catalytic activity of the Pd1 catalyst after the reduction. It was noted that NO was not converted on the Pd1 catalyst (without reduction pre-treatment) at 200 °C but it was reduced to N_2O/N_2 on the pre-reduced Pd1 catalyst at this temperature (Fig. S3). These results suggest that metallic Pd is more active than the PdO in the reduction of NO. However, when the temperature was higher than 200 °C, the metallic Pd was re-oxidized and as a result, both the Pd1 and the pre-reduced Pd1 exhibited a similar activity for NO

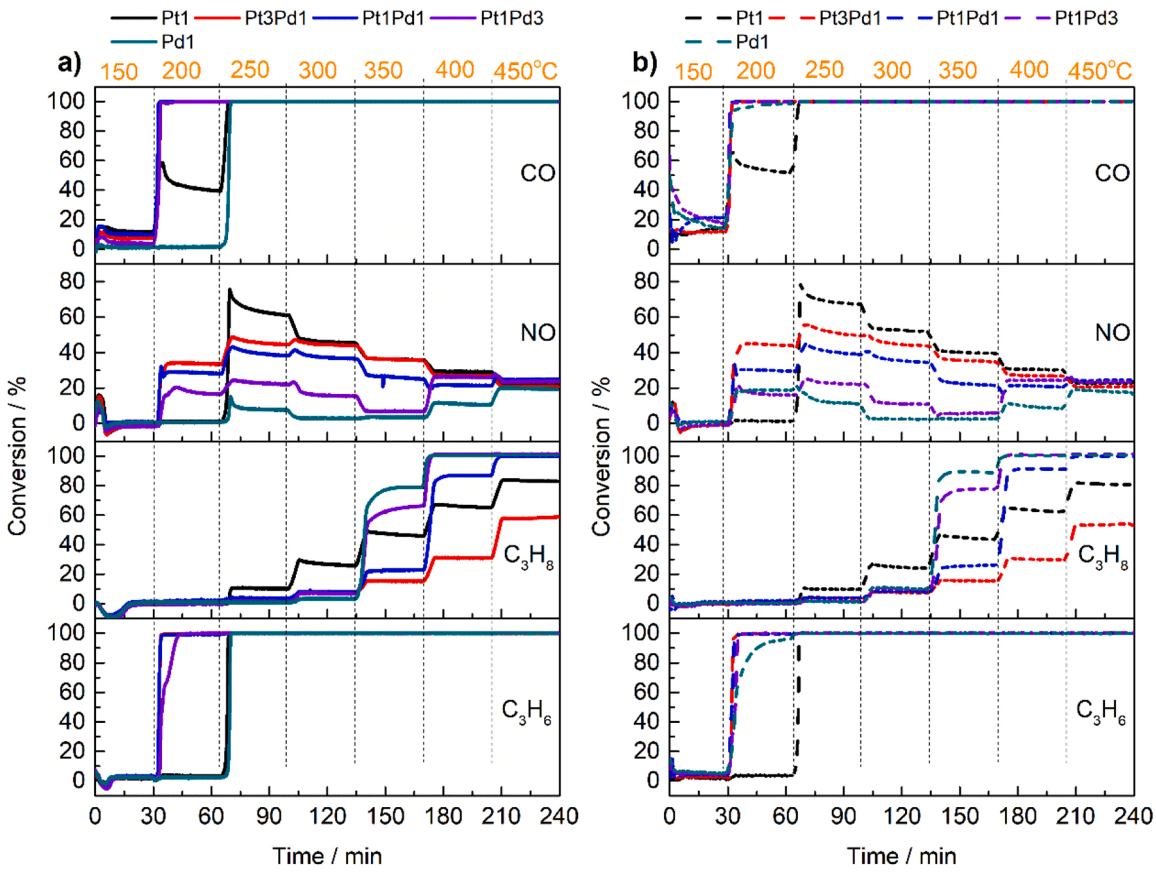

Fig. 10. The conversions of CO, NO, C_3H_8, and C_3H_6 on Pt-Pd/zeolites at 150–450 °C. The catalysts were pretreated a) without and b) with H_2 prior to the activity test. Gas composition CO (1000 ppm), NO (500 ppm), C_3H_6 (500 ppm), C_3H_8 (500 ppm), O_2 (10 %), and H_2O (5 %) balanced in Ar.

conversion (Fig. S3).

For the Pt1 catalyst, the conversions of CO and NO were slightly improved but the conversion of C_3H_8 was similar or slightly lower after the reduction (compare the solid black curve (Fig. 10a) and the dashed black curve (Fig. 10b)). It was noted that for NO conversion, the Pt1 catalyst was almost inactive at temperatures lower than 200 °C. Both NO oxidation to NO_2 and NO reduction to N_2O/N_2 were catalyzed at 250 – 300 °C whereas NO oxidation only occurred from 350 to 450 °C (Fig. S4). However, it was not possible to conclude the effect of H_2 reduction for C_3H_6 oxidation, because Pt1 exhibited full conversion at 250 °C for both cases, before and after the reduction. The effect of H_2 reduction was not significant for the Pt1 catalyst because Pt existed mainly in metallic form as revealed from XRD; however, most of the surface was in the oxide phase according to the XPS data. For the bimetallic PtPd catalysts, the H_2 reduction did improve slightly the conversion in some cases, e.g. C_3H_8, but the effect was not as significant as for the Pd1 catalyst, probably due to a higher fraction of metallic form in the PtPd alloy in these catalysts. All three bimetallic catalysts could reduce NO to N_2O at 200 °C (Figs. S5–S7), behaving similarly to the pre-reduced Pd1 catalyst. Note that the Pt1 catalyst was not active for this reaction at 200 °C. Therefore, the results indicated that the active sites of the bimetallic catalysts for NO reduction at 200 °C were related to the metallic Pd in the PtPd alloy, which agreed with the XRD data.

3.2.4. Sulfur poisoning at 200 °C and regeneration

3.2.4.1. Sulfur poisoning. After the T-step tests, the reaction was kept at 200 °C and then 20 ppm of SO_2 was fed into the gas mixture for 4 h (see Fig. 11). The conversion of C_3H_8 is not shown because all samples were not active for C_3H_8 oxidation at 200 °C. The CO conversion on the Pt1 catalyst decreased by about 6 % from 38.5 % to 32.5 % in the first 45 min of SO_2 exposure and then it gradually dropped to approximately 29 % at the end of the poisoning step, and the conversion was not increased again after the SO_2 was switched off (the black line, Fig. 11a). By contrast, for the Pd1 catalyst, the CO conversion dropped instantaneously from 66 % to 6 % in the first 8 min. After that, the conversion increased slightly to about 14 % in the next 35 min before declining again to about 1 % at 90 min of time-on-stream and remained constant until the end of the poisoning step. These observations showed that Pd is substantially more susceptible to sulfur poisoning than Pt as reported in the literature for alumina-based catalysts [16,59].

The Pt1Pd3 catalyst with a high ratio of Pd showed a similar behavior as the Pd1 catalyst; however, the conversion of CO was about 9 % at the end of the poisoning step likely due to the contribution of the Pt active sites, and the conversion was slightly increased after the SO_2 feed was stopped. The Pt1Pd1 and Pt3Pd1 exhibited similar behavior for CO conversion. Both Pt1Pd1 and Pt3Pd1 catalysts retained a full conversion of CO for the first 35 min and 45 min of the SO_2 exposure, respectively. After that, the CO conversion declined quickly during the first 90 min of the poisoning step and this was followed by a gradual decrease. The conversion of CO was approximately 31 % and 24 % for the Pt3Pd1 and Pt1Pd1, respectively, at the end of the poisoning. The large decrease in the CO conversion for both bimetallic catalysts might be related to the fast poisoning of the Pd sites, which was similar to that of the Pd1 catalyst. It should be noted that these catalysts were designed to have the same number of moles of noble metals. Interestingly, the Pt3Pd1 showed a slightly higher conversion than the Pt1 at the end of the poisoning step although it had a lower amount of Pt active sites. Remarkably, the CO conversions increased fast after SO_2 was removed from the feed gas for the bimetallic samples, containing PtPd alloy. These results suggest that the SO_2 molecules interacted weakly with the Pd/Pt species in the PtPd alloy and hence they were easily removed from

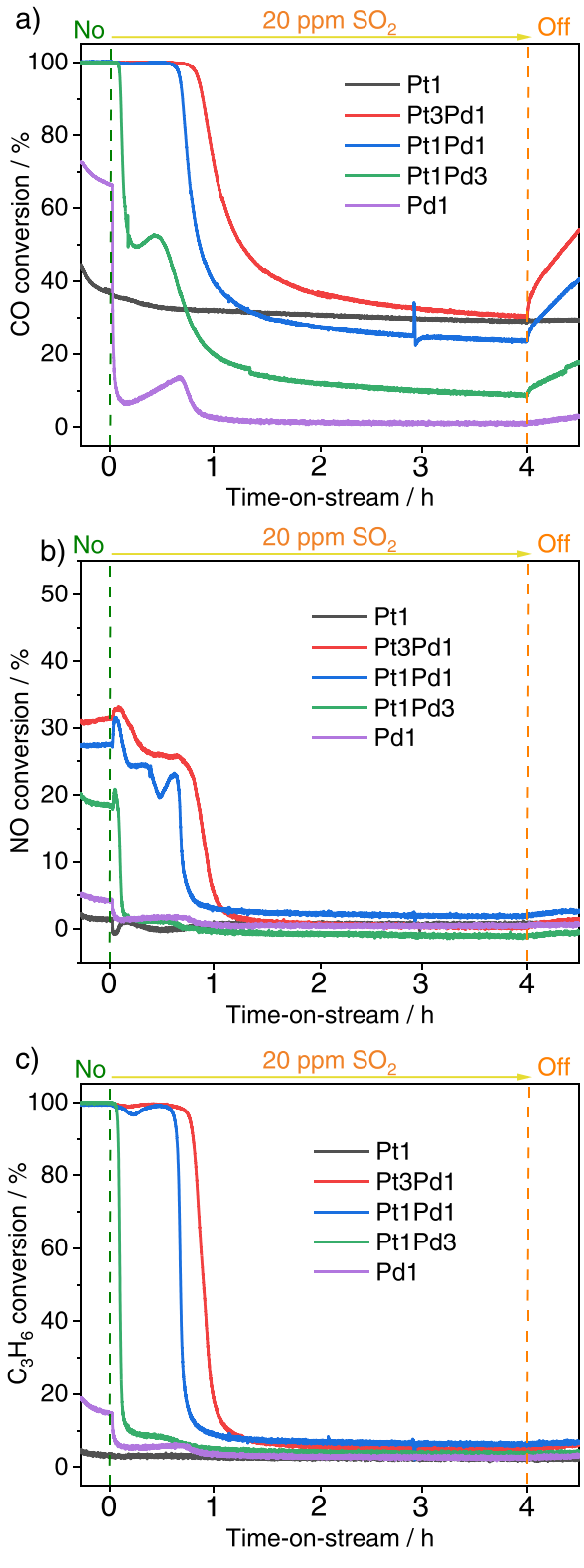

Fig. 11. Conversion profiles of CO, NO, and C_3H_6 for Pt-Pd catalysts during the SO_2 exposure (20 ppm) at 200 °C for 4 h. Gas composition CO (1000 ppm), NO (500 ppm), C_3H_6 (500 ppm), C_3H_8 (500 ppm), O_2 (10 %), and H_2O (5 %) balanced in Ar.

these sites. This behavior is very different from the monometallic catalysts. In the other words, the PtPd alloy showed more strengths for CO oxidation than the monometallic Pt under the SO_2 poisoning conditions such as better initial conversion, similar conversion after the 4 h-exposure, and faster recovery in absence of SO_2.

Another interesting point was the temporary increase in the conversion of CO with time-on-stream of SO_2 exposure at 25 and 40 min for the Pt1Pd3 and Pd1 catalysts, respectively. We note that the sulfur poisoning step was performed right after the T-step test, where the samples were pre-treated by the reduction in H_2. The formation of metallic Pd accounted for a substantial increase in the oxidation activity of the Pd1 for CO, NO, C_3H_8, and C_3H_6 as shown in Fig. 10. When comparing the CO conversion at 200 °C for the Pd1 catalyst, for example, the CO conversion at 200 °C was 1.9 %, 98.3 %, and 66.5 % in the T-step test after the catalyst had been treated in the lean condition, the reduction with H_2, and before being exposed to 20 ppm of SO_2, respectively (Fig. S8). This indicated that the metallic Pd species were only partially oxidized after the T-step test and the remaining high fraction of metallic Pd species resulted in a high conversion of CO before SO_2 exposure. After the catalyst was exposed to SO_2, the metallic Pd sites were probably interacting both with SO_2 and with O_2. The former caused a fast decline in CO conversion due to poisoning, while the latter led to an increase in the ratio of PdO_x/Pd. It has been reported in the literature that an optimum PdO_x/Pd ratio could have higher activity for CO oxidation than either PdO_x or fully metallic Pd [60,61]. We, therefore, hypothesize that a certain ratio of PdO_x/Pd with time-on-stream of SO_2 exposure accounted for the local peak in the CO conversion of the Pd1 catalyst. Similar behavior was observed for the Pt1Pd3 catalyst, which could be explained in the same way due to the high fraction of Pd in this catalyst. We note that this phenomenon was not observed for Pt1Pd1 and Pt3Pd1 because both catalysts showed 100 % conversion of CO in the initial phase of the poisoning.

For NO conversion, both Pd1 and Pt1Pd3 were quickly deactivated after being exposed to SO_2 because these catalysts had a high content of Pd which was susceptible to SO_2 poisoning (Fig. 11b). The Pt1 catalyst was not active for NO oxidation at 200 °C (the black curve) which was consistent with the data of the T-step test reported in Fig. 10. For the bimetallic catalysts containing high Pt content, i.e. Pt1Pd1 and Pt3Pd1, the duration before deactivation was prolonged; however, the conversion of NO was lower than 5 % after 1 h of SO_2 exposure to the catalysts. It was noted that NO was predominantly reduced rather than oxidized on the Pt1Pd1 and Pt3Pd1catalysts at 200 °C, and this led to forming approximately 35–45 ppm of N_2O during the test (Fig. S8).

The trend in the conversion of C_3H_6 was similar to CO oxidation for each catalyst (Fig. 11c); however, the impact of SO_2 on the C_3H_6 oxidation was more severe than for the CO oxidation. All catalysts exhibited a C_3H_6 conversion of less than 10 % after 1 h of SO_2 exposure. The Pt1 catalyst was not active enough to observe the impact of SO_2 because the conversion of C_3H_6 was negligible at 200 °C, like that for the NO oxidation. The catalysts rich in Pd (Pd1 and Pt1Pd3) quickly dropped in conversion whereas the Pt rich catalysts (Pt1Pd1 and Pt3Pd1) retained a high conversion (almost 100 %) for 35 and 45 min for Pt1Pd1 and Pt3Pd1, respectively. A local peak in the conversion of C_3H_6 for Pd1, Pt1Pd1, and Pt1Pd3 was observed, similar to the case during CO oxidation. We also hypothesize that this change in the C_3H_6 conversion was due to variation of the PdO_x/Pd ratio during the addition of SO_2.

3.2.4.2. Evaluation of SO_2 impact and regeneration. During the 4-hour exposure to SO_2 in the poisoning experiment at 200 °C, we monitored the online impact of SO_2 on CO and C_3H_6 oxidation and NO oxidation/reduction. The selected temperature was 200 °C to simulate the low temperature of the exhaust gas from diesel engines. However, the temperature was not high enough to evaluate the impact of SO_2 on the oxidation of C_3H_8. Consequently, a T-step test (150–450 °C, 50 °C intervals, 30 min each step) was performed after the sulfur poisoning step to explore the impact of SO_2 on the conversion of C_3H_8. After that, the catalyst was regenerated under two different conditions, namely, the lean reaction gas mixture at 600 °C, and the second regeneration was a reduction in 2 % H_2 in Ar. Another T-step test was performed after each

regeneration step to evaluate the recovery of the catalyst. A full set of data is reported in the SI (Figs. S10–S13). The data for the Pt1 catalyst can be found in our earlier publication [32].

Due to the brevity, we selected a typical temperature for each gas component to compare the impact of SO_2 as well as the efficiency of the regeneration process. The basis of the selection is that the conversion of the gas component should be high enough to but not reach 100 % at the selected temperature to observe the impact of SO_2 and regeneration. Fig. 12 presents the conversion of CO at 150 °C, NO at 250 °C, C_3H_6 at 200 °C, and C_3H_8 at 350 °C for each catalyst. The impact of SO_2 is significantly different not only for each gas component but also for the Pt/Pd ratio (Fig. 12). In general, SO_2 caused a decrease in the conversion of CO, NO, and C_3H_6. In the case of C_3H_8, the SO_2 exposure promoted the conversion of C_3H_8 on the Pt1 and Pt3Pd1 catalysts whereas it caused a poisoning effect for Pt1Pd1, Pt1Pd3, and Pd1 catalysts (Fig. 12d). For monometallic catalysts, the Pd1 catalyst was more susceptible to SO_2 poisoning than the Pt1 and this trend is similar to the behavior of alumina-based catalysts in the literature [2]. For example, after the sulfur poisoning step, the Pd1 and the Pt1 lost 96 % and 67 % of the CO conversion at 150 °C, respectively (compare the green and the violet bar in Fig. 11a). A severe poisoning effect on the Pd1 was also observed for C_3H_6 oxidation with a decrement of 96 % in the conversion (Fig. 12c).

NO was converted by both NO oxidation and NO reduction at 250 °C, which was associated with the formation of NO_2 and N_2O/N_2, respectively. Detailed profiles of NO_2 and N_2O concentration during this T-step test are shown in Fig. S14. At 250 °C, the effect of sulfur poisoning on NO conversion for the Pt1 and Pd1 catalysts was not significant (Fig. 12b). Furthermore, for C_3H_8 oxidation, the Pd1 lost 92 % of C_3H_8 conversion while the Pt1 gained 11 % of the C_3H_8 conversion at 350 °C (Fig. 12d). The beneficial impact of SO_2 on the oxidation of C_3H_8 has been reported in the literature for Pt/Al_2O_3 catalyst and Pt/BEA due to the enhancement of C_3H_8 adsorption/dissociation in the presence of sulfur [62–64]. This promotion effect was more pronounced for the Pt3Pd1 catalyst with an increment of 75 % of the C_3H_8 conversion. However, with the samples containing higher Pd ratios, the activity was decreased, e.g. 10 % and 77 % for Pt1Pd1 and Pt1Pd3, respectively. For the bimetallic catalysts, SO_2 poisoning caused a significant decrease in the conversion of CO, NO, and C_3H_6. The loss of the activity for NO oxidation and/or reduction and C_3H_6 oxidation was more pronounced with an increase in the Pd content (Fig. 12b and c). In summary, for monometallic catalysts, Pd is more susceptible to SO_2 than Pt and subsequently, the bimetallic PtPd catalysts containing higher contents of Pd are also more sensitive to SO_2 poisoning. Interestingly, a small fraction of Pd can stimulate the promotional effect of SO_2 on C_3H_8 oxidation, e.g. the Pt3Pd1; however, increasing further the fraction of Pd caused a negative effect due to the sensitivity of Pd to SO_2 poisoning.

Regeneration in lean conditions is of large practical interest since the exhaust gas from diesel vehicles is lean. The first regeneration condition (R1) is therefore in a lean gas mixture at 600 °C. However, it is challenging to remove sulfur under lean conditions, and thus the second regeneration in rich conditions with H_2 was also examined (R2). The recovery degree is reported in Table S1. The deactivation of the catalysts

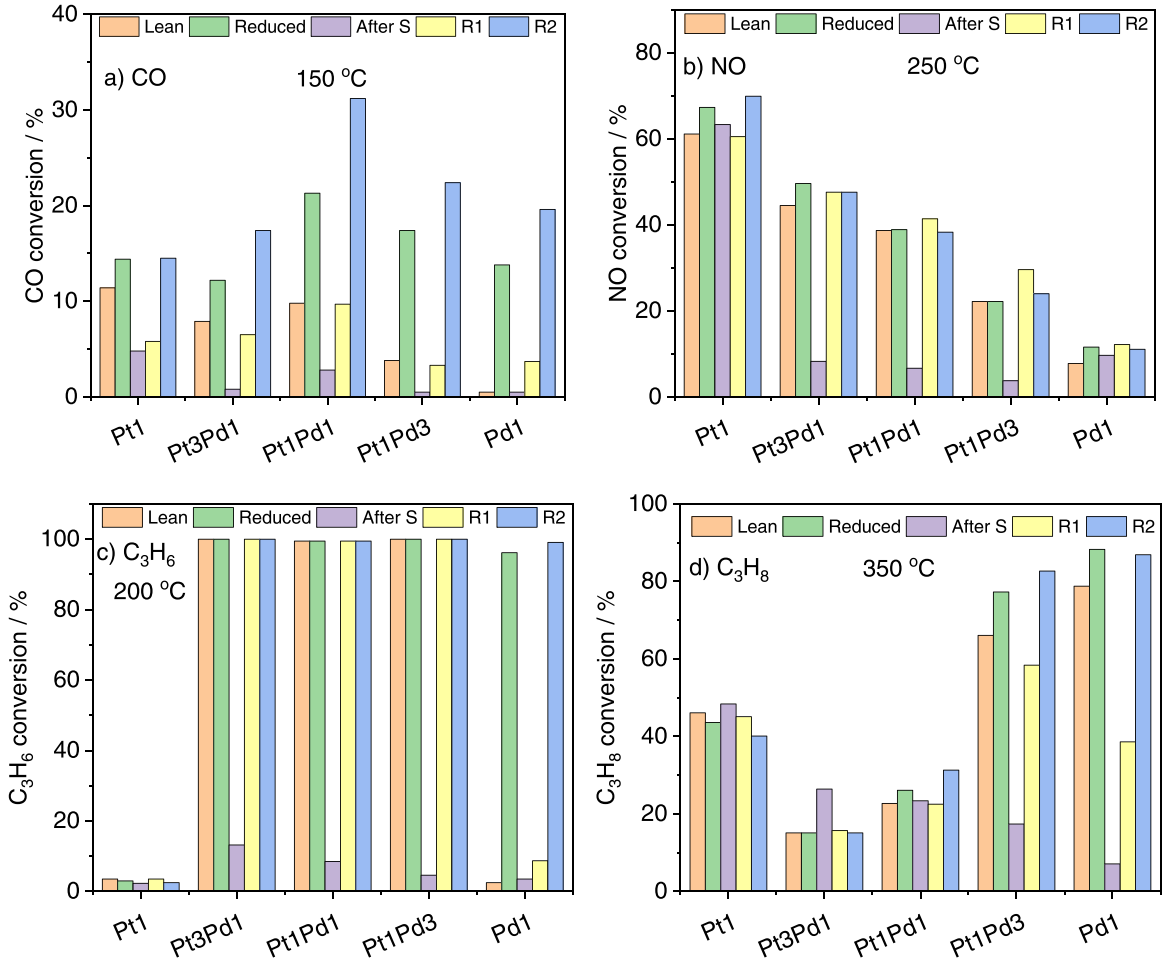

Fig. 12. Comparison of conversion of a) CO (150 °C), b) NO (250 °C), and c) C_3H_6 (200 °C), and C_3H_8 (350 °C) for different catalysts at different temperatures through T-step experiments after poisoning with SO_2 at 200 °C: Lean conditions (before the treatment with H_2, orange bar), reduced conditions (after the treatment with H_2) and before SO_2 addition (green bar), after SO_2 addition (after S, violet bar), after regeneration in lean conditions R1 (yellow bar), and after regeneration with hydrogen R2 (blue bar).

during the exposure to SO_2 could be related to either coverage of the metallic phase (Pt/Pd) with SO_2 or the induced oxidation of Pt/Pd with SO_2. In the case of Pd, the PdO phase can react with SO_2 to form sulfite or sulfate which accounted for a faster deactivation of the Pd-based catalyst than the Pt counterparts [58,65]. Reduction with H_2 (R2) was more efficient to regenerate the Pd1 catalyst for oxidation of CO, C_3H_6, and C_3H_8 than thermal treatment under the lean condition (R1) because it is more effective to remove sulfur in an H_2 atmosphere. In addition, the metallic Pd species were more active than PdO for these reactions and this is another beneficial effect of R2 (Table S1). For the Pt1 and the bimetallic catalysts, both R1 and R2 efficiently regenerated the activity for the oxidation of NO and C_3H_6. However, R2 was more efficient than R1 to regenerate the Pt1 and the bimetallic catalysts for CO oxidation, which also was the case for Pt1Pd1 and Pt1Pd3 for C_3H_8.

4. Conclusions

A series of PtPd catalysts with different ratios of Pt/Pd supported on high siliceous BEA zeolite ($SiO_2/Al_2O_3 = 217$) have been prepared by incipient impregnation, characterized, and tested as diesel oxidation catalysts. The alloy of Pt and Pd was formed in the cases of the bimetallic catalysts as indicated from XRD analysis. The particle sizes of the noble metals in the bimetallic samples (7–12 nm) after high-temperature degreening (700 °C) were slightly smaller than that of the Pt monometallic catalyst (16 nm) because the Pt-Pd alloy prevented the sintering of the noble metal particles. Moreover, the formation of the Pt-Pd alloy retained more species of Pd in a lower oxidation state. All three bimetallic catalysts showed a significant improvement in the oxidation of CO and C_3H_6. These bimetallic catalysts also shifted the reduction of NO to lower light-off temperature, although the absolute values of the maximum conversions were lower than that for the monometallic Pt1 due to a lower amount of Pt loading. For monometallic catalysts, Pt was more resistant to sulfur poisoning than Pd, which is consistent with the behavior of Pt/Al_2O_3 and Pd/Al_2O_3 catalysts, although the catalysts in the present work employed high siliceous beta zeolite as support. The bimetallic PtPd catalysts not only delayed the deactivation time by SO_2 but also retained better performance than the Pd1 throughout the poisoning period. Pt1 catalyst exhibited less deactivation for CO oxidation, but the initial activity prior to sulfur poisoning and also after was significantly lower than the bimetallic samples. Thermal treatment in lean conditions can regenerate the activity for NO and C_3H_6 oxidation on bimetallic catalysts but a reduction in H_2 is necessary to recover the activity for CO and C_3H_8 oxidation.

CRediT authorship contribution statement

Phuoc Hoang Ho: Conceptualization, Investigation, Formal analysis, Writing – original draft. **Jieling Shao:** Formal analysis, Writing – review & editing. **Dawei Yao:** Investigation, Writing – review & editing. **Rojin Feizie Ilmasani:** Investigation, Writing – review & editing. **Muhammad Abdus Salam:** Investigation, Writing – review & editing. **Derek Creaser:** Conceptualization, Supervision, Writing – review & editing. **Louise Olsson:** Conceptualization, Supervision, Writing – review & editing, Funding acquisition.

Declaration of Competing Interest

The authors declare that they have no known competing financial interests or personal relationships that could have appeared to influence the work reported in this paper.

Acknowledgements

This study has been funded by the Swedish Energy Agency, Johnson Matthey, and Volvo AB via the FFI project (Grant number 48038-1). We would like to acknowledge Dr. Gudmund Smedler, Dr. Francois Moreau, Dr. Andrew Chiffey (Johnson Matthey) and Dr. Lennart Andersson, Dr. Martin Petersson (Volvo AB) for valuable comments and discussions. We also appreciate the assistance of Dr. Eric Tam (XPS analysis), Dr. Stefan Gustafsson (TEM measurements), and Dr. Andreas Schaefer (CO chemisorption).

Appendix A. Supporting information

Supplementary data associated with this article can be found in the online version at doi:10.1016/j.jece.2022.108217.

References

[1] R.J. Farrauto, K.E. Voss, Monolithic diesel oxidation catalysts, Appl. Catal. B Environ. 10 (1996) 29–51.
[2] A. Russell, W.S. Epling, Diesel oxidation catalysts, Catal. Rev. 53 (2011) 337–423.
[3] J.E. Etheridge, T.C. Watling, A.J. Izzard, M.A.J. Paterson, The effect of Pt:Pd ratio on light-duty diesel oxidation catalyst performance: an experimental and modelling study, SAE Int. J. Engines 8 (2015) 1283–1299.
[4] K. Kallinen, A. Moreno, A. Savimäki, T.-J.J. Kinnunen, Pt/Pd diesel oxidation catalyst: a study on the properties enhanced by the use of Pd, SAE Tech. Pap. (2009) 2009–26–0018, https://doi.org/10.4271/2009-26-0018.
[5] L. Glover, R. Douglas, G. McCullough, M. Keenan, P. Revereault, C. McAtee, Performance characterisation of a range of diesel oxidation catalysts: effect of Pt:Pd ratio on light off behaviour and nitrogen species formation, SAE Tech. Pap. (2011) 2011–24–0193, https://doi.org/10.4271/2011-24-0193.
[6] T.C. Watling, M. Ahmadinejad, M. Ţuţuianu, Å. Johansson, M.A.J. Paterson, Development and validation of a Pt-Pd diesel oxidation catalyst model, SAE Int. J. Engines 5 (2012) 1420–1442.
[7] J. Li, A. Kumar, X. Chen, N. Currier, A. Yezerets, Impact of different forms of sulfur poisoning on diesel oxidation catalyst performance, SAE Tech. Pap. (2013) 2013–01-0514, https://doi.org/10.4271/2013-01-0514.
[8] B.M. Shakya, B. Sukumar, Y.M. López-De Jesús, P. Markatou, The effect of Pt:Pd ratio on heavy-duty diesel oxidation catalyst performance: an experimental and modeling study, SAE Int. J. Engines 8 (2015) 1271–1282.
[9] M. Agote-Arán, M. Elsener, F.W. Schütze, C.M. Schilling, M. Sridhar, E. Katsaounis, O. Kröcher, D. Ferri, Understanding the impact of poison distribution on the performance of Diesel oxidation catalysts, Appl. Catal. B Environ. 299 (2021), 120684.
[10] A. Gremminger, J. Pihl, M. Casapu, J.-D. Grunwaldt, T.J. Toops, O. Deutschmann, PGM based catalysts for exhaust-gas after-treatment under typical diesel, gasoline and gas engine conditions with focus on methane and formaldehyde oxidation, Appl. Catal. B Environ. 265 (2020), 118571.
[11] J. Kim, Y. Kim, M.H. Wiebenga, S.H. Oh, D.H. Kim, Oxidation of C_3H_8, iso-C_5H_{12} and C_3H_6 under near-stoichiometric and fuel-lean conditions over aged Pt–Pd/Al_2O_3 catalysts with different Pt:Pd ratios, Appl. Catal. B Environ. 251 (2019) 283–294.
[12] H. Xiong, E. Peterson, G. Qi, A.K. Datye, Trapping mobile Pt species by PdO in diesel oxidation catalysts: smaller is better, Catal. Today 272 (2016) 80–86.
[13] M.J. Hazlett, M. Moses-Debusk, J.E. Parks, L.F. Allard, W.S. Epling, Kinetic and mechanistic study of bimetallic Pt-Pd/Al_2O_3 catalysts for CO and C_3H_6 oxidation, Appl. Catal. B Environ. 202 (2017) 404–417.
[14] M. Haneda, K. Suzuki, M. Sasaki, H. Hamada, M. Ozawa, Catalytic performance of bimetallic PtPd/Al_2O_3 for diesel hydrocarbon oxidation and its implementation by acidic additives, Appl. Catal. A Gen. 475 (2014) 109–115.
[15] A. Morlang, U. Neuhausen, K.V. Klementiev, F.W. Schütze, G. Miehe, H. Fuess, E. S. Lox, Bimetallic Pt/Pd diesel oxidation catalysts: structural characterisation and catalytic behaviour, Appl. Catal. B Environ. 60 (2005) 191–199.
[16] P.H. Ho, J.-W. Woo, R. Feizie Ilmasani, J. Han, L. Olsson, The role of Pd–Pt interactions in the oxidation and sulfur resistance of bimetallic Pd–Pt/γ-Al_2O_3 diesel oxidation catalysts, Ind. Eng. Chem. Res. 60 (2021) 6596–6612.
[17] X. Auvray, L. Olsson, Stability and activity of Pd-, Pt- and Pd–Pt catalysts supported on alumina for NO oxidation, Appl. Catal. B Environ. 168–169 (2015) 342–352.
[18] C.H. Kim, M. Schmid, S.J. Schmieg, J. Tan, W. Li, The effect of Pt-Pd ratio on oxidation catalysts under simulated diesel exhaust, SAE Int. (2011) 2011–01-1134, https://doi.org/10.4271/2011-01-1134.
[19] W. Yang, J. Gong, X. Wang, Z. Bao, Y. Guo, Z. Wu, A review on the impact of SO_2 on the oxidation of NO, hydrocarbons, and CO in Diesel emission control catalysis, ACS Catal. (2021) 12446–12468.
[20] J. Zhang, D. Lou, Y. Sun, P. Tan, Z. Hu, C. Huang, Effects of DOC and CDPF catalyst composition on emission characteristics of light-duty diesel engine with DOC + CDPF + SCR system, SAE Tech. Pap. (2018) 2018–01-0337, https://doi.org/10.4271/2018-01-0337.
[21] M. Skoglundh, L.O. Löwendahl, J.E. Otterated, Combinations of platinum and palladium on alumina supports as oxidation catalysts, Appl. Catal. 77 (1991) 9–20.
[22] S.B. Kang, M. Hazlett, V. Balakotaiah, C. Kalamaras, W. Epling, Effect of Pt:Pd ratio on CO and hydrocarbon oxidation, Appl. Catal. B Environ. 223 (2018) 67–75.
[23] M. Han, D. Assanis, S. Bohac, Characterization of heat-up diesel oxidation catalysts through gas flow reactor and in-situ engine testing, Proc. Inst. Mech. Eng., Part D J. Automob. Eng. 222 (2008) 1705–1716.
[24] J. Sawyer, J. Summers, Treatment of Diesel Exhaust Gas Using Zeolite Catalyst US5849255, 1998.

[25] G. Ansell, J. Fisher, H. Hamilton, R.R. Rajaram, Diesel Engine Exhaust Gas Purification Method US5943857, 1999.

[26] Y. Gu, W.S. Epling, Passive NOx adsorber: an overview of catalyst performance and reaction chemistry, Appl. Catal. A Gen. 570 (2019) 1–14.

[27] B. Moden, J.M. Donohue, W.E. Cormier, H.-X. Li, The uses and challenges of zeolites in automotive applications, Top. Catal. 53 (2010) 1367–1373.

[28] R.F. Ilmasani, P.H. Ho, A. Wang, D. Yao, D. Creaser, L. Olsson, Investigation of CO deactivation of passive NOx adsorption on La promoted Pd/BEA, Emiss. Control Sci. Technol. (2021), https://doi.org/10.1007/s40825-021-00205-2.

[29] I. Friberg, N. Sadokhina, L. Olsson, The effect of Si/Al ratio of zeolite supported Pd for complete CH_4 oxidation in the presence of water vapor and SO_2, Appl. Catal. B Environ. 250 (2019) 117–131.

[30] I. Friberg, A.H. Clark, P.H. Ho, N. Sadokhina, G.J. Smales, J. Woo, X. Auvray, D. Ferri, M. Nachtegaal, O. Kröcher, L. Olsson, Structure and performance of zeolite supported Pd for complete methane oxidation, Catal. Today 382 (2021) 3–12.

[31] P.H. Ho, J. Woo, R.F. Ilmasani, M.A. Salam, D. Creaser, L. Olsson, The effect of Si/Al ratio on the oxidation and sulfur resistance of beta zeolite-supported Pt and Pd as diesel oxidation catalysts, ACS Eng. Au 2 (2022) 27–45.

[32] P.H. Ho, D. Creaser, L. Olsson, Advantages of high siliceous zeolites in the reactivity and stability of diesel oxidation catalysts, ACS Eng. Au (2022), https://doi.org/10.1021/acsengineeringau.1c00035.

[33] G.W. Graham, H.W. Jen, O. Ezekoye, R.J. Kudla, W. Chun, X.Q. Pan, R.W. McCabe, Effect of alloy composition on dispersion stability and catalytic activity for NO oxidation over alumina-supported Pt–Pd catalysts, Catal. Lett. 116 (2007) 1–8.

[34] S.M. Foiles, M.I. Baskes, M.S. Daw, Embedded-atom-method functions for the fcc metals Cu, Ag, Au, Ni, Pd, Pt, and their alloys, Phys. Rev. B 33 (1986) 7983–7991.

[35] M. Kaneeda, H. Iizuka, T. Hiratsuka, N. Shinotsuka, M. Arai, Improvement of thermal stability of NO oxidation Pt/Al_2O_3 catalyst by addition of Pd, Appl. Catal. B Environ. 90 (2009) 564–569.

[36] D. Kubička, N. Kumar, T. Venäläinen, H. Karhu, I. Kubičková, H. Österholm, D. Y. Murzin, Metal−support interactions in zeolite-supported noble metals: influence of metal crystallites on the support acidity, J. Phys. Chem. B 110 (2006) 4937–4946.

[37] J. Liu, H. Zhang, N. Lu, X. Yan, B. Fan, R. Li, Influence of acidity of mesoporous ZSM-5-supported Pt on naphthalene hydrogenation, Ind. Eng. Chem. Res. 59 (2020) 1056–1064.

[38] L.K. Ono, B. Yuan, H. Heinrich, B.R. Cuenya, Formation and thermal stability of platinum oxides on size-selected platinum nanoparticles: support effects, J. Phys. Chem. C 114 (2010) 22119–22133.

[39] J.F. Moulder, J. Chastain. Handbook of X-ray Photoelectron Spectroscopy: a Reference Book of Standard Spectra for Identification and Interpretation of XPS Data, Physical Electronics Division, Perkin-Elmer Corporation, Minnesota, 1992, pp. 110–152.

[40] L. Olsson, E. Fridell, The influence of Pt oxide formation and Pt dispersion on the reactions $NO_2 \Leftrightarrow NO+1/2\ O_2$ over Pt/Al_2O_3 and $Pt/BaO/Al_2O_3$, J. Catal. 210 (2002) 340–353.

[41] J. Oenema, J.P. Hofmann, E.J.M. Hensen, J. Zečević, K.P. de Jong, Assessment of the location of Pt nanoparticles in Pt/zeolite Y/γ-Al_2O_3 composite catalysts, ChemCatChem 12 (2020) 615–620.

[42] M.-F. Luo, Z.-Y. Hou, X.-X. Yuan, X.-M. Zheng, Characterization study of CeO_2 supported Pd catalyst for low-temperature carbon monoxide oxidation, Catal. Lett. 50 (1998) 205–209.

[43] Y. Zheng, L. Kovarik, M.H. Engelhard, Y. Wang, Y. Wang, F. Gao, J. Szanyi, Low-temperature Pd/Zeolite passive NOx adsorbers: structure, performance, and adsorption chemistry, J. Phys. Chem. C 121 (2017) 15793–15803.

[44] T.R. Johns, J.R. Gaudet, E.J. Peterson, J.T. Miller, E.A. Stach, C.H. Kim, M. P. Balogh, A.K. Datye, Microstructure of bimetallic Pt-Pd Catalysts under oxidizing conditions, ChemCatChem 5 (2013) 2636–2645.

[45] M. Rivallan, E. Seguin, S. Thomas, M. Lepage, N. Takagi, H. Hirata, F. Thibault-Starzyk, Platinum sintering on H-ZSM-5 followed by chemometrics of CO adsorption and 2D pressure-jump IR spectroscopy of adsorbed species, Angew. Chem. Int. Ed. 49 (2010) 785–789.

[46] H. Bischoff, N.I. Jaeger, G. Schulz-Ekloff, L. Kubelkova, Interaction of CO with platinum species in zeolites. Evidence for platinum carbonyls in partially reduced zeolite PtNaX, J. Mol. Catal. 80 (1993) 95–103.

[47] B.L. Mojet, J.T. Miller, D.E. Ramaker, D.C. Koningsberger, A. New, Model describing the metal–support interaction in noble metal catalysts, J. Catal. 186 (1999) 373–386.

[48] I.V. Yudanov, R. Sahnoun, K.M. Neyman, N. Rösch, J. Hoffmann, S. Schauermann, V. Johánek, H. Unterhalt, G. Rupprechter, J. Libuda, H.-J. Freund, CO adsorption on Pd nanoparticles: density functional and vibrational spectroscopy studies, J. Phys. Chem. B 107 (2003) 255–264.

[49] E.K. Dann, E.K. Gibson, R.A. Catlow, P. Collier, T. Eralp Erden, D. Gianolio, C. Hardacre, A. Kroner, A. Raj, A. Goguet, P.P. Wells, Combined in situ XAFS/DRIFTS studies of the evolution of nanoparticle structures from molecular precursors, Chem. Mater. 29 (2017) 7515–7523.

[50] K. Chakarova, E. Ivanova, K. Hadjiivanov, D. Klissurski, H. Knözinger, Co-ordination chemistry of palladium cations in Pd-H-ZSM-5 as revealed by FTIR spectra of adsorbed and co-adsorbed probe molecules (CO and NO), Phys. Chem. Chem. Phys. 006 (2004) 3702–3709.

[51] H. Dubbe, G. Eigenberger, U. Nieken, Hysteresis phenomena on Pt- and Pd-diesel oxidation catalysts: experimental observations, Top. Catal. 59 (2016) 1054–1058.

[52] D. Yao, R.F. Ilmasani, J.C. Wurzenberger, T. Glatz, J. Han, P.H. Ho, D. Creaser, L. Olsson, Insight into CO induced degradation mode of Pd/SSZ-13 in NO_x adsorption and release: experiment and modeling, Chem. Eng. J. 439 (2022), 135714.

[53] L. Glover, R. Douglas, G. McCullough, M. Keenan, P. Revereault, C. McAtee, Performance characterisation of a range of diesel oxidation catalysts: effect of Pt:Pd ratio on light off behaviour and nitrogen species formation, SAE Int., Tech. Pap. (2011), 24-0193, https://doi.org/10.4271/2011-24-0193.

[54] J.E. Etheridge, T.C. Watling, A.J. Izzard, M.A.J. Paterson, The effect of Pt:Pd ratio on light-duty diesel oxidation catalyst performance an experimental and modelling study, SAE Int. J. Engines 8 (2015) 1283–1299.

[55] Z. Zhang, M. Chen, Z. Jiang, W. Shangguan, Low-temperature selective catalytic reduction of NO with propylene in excess oxygen over the Pt/ZSM-5 catalyst, J. Hazard. Mater. 193 (2011) 330–334.

[56] M. Khosravi, C. Sola, A. Abedi, R.E. Hayes, W.S. Epling, M. Votsmeier, Oxidation and selective catalytic reduction of NO by propene over Pt and Pt:Pd diesel oxidation catalysts, Appl. Catal. B Environ. 147 (2014) 264–274.

[57] T. Komatsu, K. Tomokuni, I. Yamada, Outstanding low temperature HC-SCR of NOx over platinum-group catalysts supported on mesoporous materials expecting diesel-auto emission regulation, Catal. Today 116 (2006) 244–249.

[58] L. Kiwi-Minsker, I. Yuranov, E. Slavinskaia, V. Zaikovskii, A. Renken, Pt and Pd supported on glass fibers as effective combustion catalysts, Catal. Today 59 (2000) 61–68.

[59] H.N. Sharma, V. Sharma, A.B. Mhadeshwar, R. Ramprasad, Why Pt survives but Pd suffers from SOx poisoning? J. Phys. Chem. Lett. 6 (2015) 1140–1148.

[60] K. Zorn, S. Giorgio, E. Halwax, C.R. Henry, H. Grönbeck, G. Rupprechter, CO oxidation on technological $Pd-Al_2O_3$ catalysts: oxidation state and activity, J. Phys. Chem. C 115 (2011) 1103–1111.

[61] Y. Zhang, Y. Cai, Y. Guo, H. Wang, L. Wang, Y. Lou, Y. Guo, G. Lu, Y. Wang, The effects of the Pd chemical state on the activity of Pd/Al_2O_3 catalysts in CO oxidation, Catal. Sci. Technol. 4 (2014) 3973–3980.

[62] A.F. Lee, K. Wilson, R.M. Lambert, C.P. Hubbard, R.G. Hurley, R.W. McCabe, H. S. Gandhi, The origin of SO_2 promotion of propane oxidation over Pt/Al_2O_3 catalysts, J. Catal. 184 (1999) 491–498.

[63] M. Skoglundh, A. Ljungqvist, M. Petersson, E. Fridell, N. Cruise, O. Augustsson, E. Jobson, SO_2 promoted oxidation of ethyl acetate, ethanol and propane, Appl. Catal. B Environ. 30 (2001) 315–328.

[64] G. Corro, R. Montiel, C. Vázquez, L, Promoting and inhibiting effect of SO_2 on propane oxidation over Pt/Al_2O_3, Catal. Commun. 3 (2002) 533–539.

[65] M.S. Wilburn, W.S. Epling, SO_2 adsorption and desorption characteristics of bimetallic Pd-Pt catalysts: Pd:Pt ratio dependency, Catal. Today 320 (2019) 11–19.